[3] Gilhar A, Kalish RS. Alopecia areata: a tissue specific autoimmune disease of the hair follicle. Autoimmun Rev 2006;5:64–9.
[4] Alkhalifah A, Alsantali A, Wang E, McElwee KJ, Shapiro J. Alopecia areata update: part I. Clinical picture, histopathology, and pathogenesis. J Am Acad Dermatol 2010;62:177–88.
[5] Paus R, Slominski A, Czarnetzki BM. Is alopecia areata an autoimmune-response against melanogenesis-related proteins, exposed by abnormal MHC class I expression in the anagen hair bulb? Yale J Biol Med 1993;66:541–54.
[6] Tobin DJ, Fenton DA, Kendall MD. Ultrastructural observations on the hair bulb melanocytes and melanosomes in acute alopecia areata. J Invest Dermatol 1990;94:803–7.
[7] Tobin DJ, Fenton DA, Kendall MD. Ultrastructural study of exclamation-mark hair shafts in alopecia areata. J Cutan Pathol 1990;17:348–54.
[8] Gilhar A, Landau M, Assy B, Ullmann Y, Shalaginov R, Serafimovich S, et al. Transfer of alopecia areata in the human scalp graft/Prkdc(scid) (SCID) mouse system is characterized by a TH1 response. Clin Immunol 2003;106:181–7.
[9] Gilhar A, Landau M, Assay B, Shalaginov R, Serafimovich S, Kalish RS. Melanocyte associated T-cell epitopes can function as autoantigens for transfer of alopecia areata to human scalp explants on Prkdcscid mice. J Invest Dermatol 2001;117:1357–62.
[10] Hordinsky M, Ericson M. Autoimmunity: alopecia areata. J Investig Dermatol Symp Proc 2004;9:73–8.
[11] Paus R, Ito N, Ito T. The theory of immune privilege of the hair follicle. In: Chan LS, editor. Animal model of human inflammatory skin diseases. Boca Raton: CRC Press; 2003. p. 155–65.
[12] Paus R, Ito N, Takigawa M, Ito T. The hair follicle and immune privilege. J Investig Dermatol Symp Proc 2003;8:188–94.
[13] Paus R, Nickoloff BJ, Ito T. A 'hairy' privilege. Trends Immunol 2005;26:32–40.
[14] Ito T, Ito N, Bettermann A, Tokura Y, Takigawa M, Paus R. Collapse and restoration of MHC class-I-dependent immune privilege: exploiting the human hair follicle as a model. Am J Pathol 2004;164:623–34.
[15] Ito T, Ito N, Saatoff M, Hashizume H, Fukamizu H, Nickoloff BJ, et al. Maintenance of hair follicle immune privilege is linked to prevention of NK cell attack. J Invest Dermatol 2008;128:1196–206.
[16] Ito T, Takigawa M. Immune privilege and alopecia areata. Exp Rev Dermatol 2010;5:141–8.
[17] Bröcker EB, Echternacht-Happle K, Hamm H, Happle R. Abnormal expression of class I and class II major histocompatibility antigens in alopecia areata: modulation by topical immunotherapy. J Invest Dermatol 1987;88:564–8.
[18] Paus R, Christoph T, Müller-Röver S. Immunology of the hair follicle: a short journey into terra incognita. J Investig Dermatol Symp Proc 1999;4:226–34.
[19] Welker P, Foitzik K, Bulfone-Paus S, Henz BM, Paus R. Hair cycle-dependent changes in the gene expression and protein content of transforming factor beta 1 and beta 3 in murine skin. Arch Dermatol Res 1997;289:554–7.
[20] Slominski A, Wortsman J, Mazurkiewicz JE, Matsuoka L, Dietrich J, Lawrence K, et al. Detection of proopiomelanocortin-derived antigens in normal and pathologic human skin. J Lab Clin Med 1993;122:658–66.
[21] Botchkarev VA, Botchkareva NV, Slominski A, Roloff B, Luger T, Paus R. Developmentally regulated expression of alpha-MSH and MC-1 receptor in C57BL/6 mouse skin suggests functions beyond pigmentation. Ann N Y Acad Sci 1999;885:433–9.
[22] Weedon D. Diseases of cutaneous appendages. In: Weedon D, editor. Weedon's skin pathology. London: Churchill Livingstone; 2002.
[23] Todes-Taylor N, Turner R, Wood GS, Stratte PT, Morhenn VB. T cell subpopulations in alopecia areata. J Am Acad Dermatol 1984;11:216–23.
[24] Arca E, Muşabak U, Akar A, Erbil AH, Taştan HB. Interferon-gamma in alopecia areata. Eur J Dermatol 2004;14:33–6.
[25] Gilhar A, Kam Y, Assy B, Kalish RS. Alopecia areata induced in C3H/HeJ mice by interferon-gamma: evidence for loss of immune privilege. J Invest Dermatol 2005;124:288–9.
[26] Benoit S, Toksoy A, Goebeler M, Gillitzer R. Selective expression of chemokine monokine induced by interferon-gamma in alopecia areata. J Invest Dermatol 2003;121:933–5.
[27] Gregoriou S, Papafragkaki D, Kontochristopoulos G, Rallis E, Kalogeromitros D, Rigopoulos D. Cytokines and other mediators in alopecia areata. Mediators Inflamm 2010 [Epub 2010 March 1].
[28] Kuwano Y, Fujimoto M, Watanabe R, Ishiura N, Nakashima H, Ohno Y, et al. Serum chemokine profiles in patients with alopecia areata. Br J Dermatol 2007;157:466–73.
[29] Subramanya RD, Coda AB, Sinha AA. Transcriptional profiling in alopecia areata defines immune and cell cycle control related genes within disease-specific signatures. Genomics 2010;96:146–53.
[30] Olsen EA, Hordinsky MK, Price VH, Roberts JL, Shapiro J, Canfield D, et al. Alopecia areata investigational assessment guidelines – Part II. National Alopecia Areata Foundation. J Am Acad Dermatol 2004;51:440–7.
[31] Hashizume H, Hansen A, Poulsen LK, Thomsen AR, Takigawa M, Thestrup-Pedersen K. In vitro propagation and dynamics of T cells from skin biopsies by methods using interleukins-2 and -4 or anti-CD3/CD28 antibody-coated microbeads. Acta Derm Venereol 2010;90:468–73.
[32] Christoph T, Müller-Rover S, Audring H, Tobin DJ, Hermes B, Cotsarelis G, et al. The human hair immune system: cellular composition and immune privilege. Br J Dermatol 2000;142:862–73.
[33] Paré L, Marcuello E, Altés A, del Río E, Sedano L, Salazar J, et al. Pharmacogenetic prediction of clinical outcome in advanced colorectal cancer patients receiving oxaliplatin/5-fluorouracil as first-line chemotherapy. Br J Cancer 2008;99:1050–5.
[34] Hashizume H, Seo N, Ito T, Takigawa M, Yagi H. Promiscuous interaction between gold-specific T cells and APCs in gold allergy. J Immunol 2008;181:8096–102.
[35] Ito T, Ito N, Hashizume H, Takigawa M. Roxithromycin inhibits chemokine-induced chemotaxis of Th1 and Th2 cells but regulatory T cells. J Dermatol Sci 2009;54:185–91.
[36] Ito T. Advances in the management of alopecia areata. J Dermatol 2012;39:11–7.
[37] Loetscher M, Gerber B, Loetscher P, Jones SA, Piali L, Clark-Lewis I, et al. Chemokine receptor specific for IP-10 and Mig: structure, function and expression in activated T lymphocytes. J Exp Med 1996;184:963–9.
[38] Gulzar N, Diker B, Balasubramanian S, Jiang JQ, Copeland KF. Human immunodeficiency virus-1 infection protects against a Tc1-to-Tc2 shift in CD8(+) T cells. Hum Immunol 2011;72:995–1000.
[39] Caterina MJ, Devreotes PN. Molecular insights into eukaryotic chemotaxis. FASEB J 1991;15:3078–85.
[40] Bailly M, Jones GE. Polarised migration: cofilin holds the front. Curr Biol 2003;13:R128–30.
[41] Dawe HR, Minamide LS, Bamburg JR, CrAm LP. ADF/cofilin controls cell polarity during fibroblast migration. Curr Biol 2003;13:252–7.
[42] McPhee CG, Duncan FJ, Silva KA, King Jr LE, Hogenesch H, Roopenian DC, et al. Increased expression of Cxcr3 and its ligands, Cxcl9 and Cxcl10, during the development of alopecia areata in the mouse. J Invest Dermatol 2012;132:1736–8.
[43] Petukhova L, Duvic M, Hordinsky M, Norris D, Price V, Shimomura Y, et al. Genome-wide association study in alopecia areata implicates both innate and adaptive immunity. Nature 2010;466:113–7.
[44] Wenzel J, Lucas S, Zahn S, Mikus S, Metze D, Ständer S, et al. CXCR3 ligand-mediated skin inflammation in cutaneous lichenoid graft-versus-host disease. J Am Acad Dermatol 2008;58:437–42.
[45] De Panfilis G. CD8+ cytolytic T lymphocytes and the skin. Exp Dermatol 1998;7:121–31.
[46] King Jr LE, McElwee KJ, Sundberg JP. Alopecia areata. Curr Dir Autoimmun 2008;10:280–312.
[47] Gilhar A, Paus R, Kalish RS. Lymphocytes, neuropeptides, and genes involved in alopecia areata. J Clin Invest 2007;117:2019–27.
[48] Rodriguez TA, Duvic M. Onset of alopecia areata after Epstein–Barr virus infectious mononucleosis. J Am Acad Dermatol 2008;59:137–9.
[49] Ito T, Tokura Y. Alopecia areata triggered or exacerbated by swine flu virus infection. J Dermatol 2012;39:863–4.
[50] Gupta MA, Gupta AK, Watteel GN. Stress and alopecia areata: a psychodermatologic study. Acta Derm Venereol 1997;77:296–8.
[51] Ito T, Ito N, Saathoff M, Bettermann A, Takigawa M, Paus R. Interferon-gamma is a potent inducer of catagen-like changes in cultured human anagen hair follicles. Br J Dermatol 2005;152:623–31.
[52] Alkhalifah A, Alsantali A, Wang E, McElwee KJ, Shapiro J. Alopecia areata update: part II. Treatment. J Am Acad Dermatol 2010;62:191–202.
[53] Ogawa N, Ping L, Zhenjun L, Takada Y, Sugai S. Involvement of the interferon-induced T cell-attracting chemokines, interferon-inducible 10-kd protein (CXCL10) and monokine induced by interferon-(CXCL9), in the salivary gland lesions of patients with Sjögren's syndrome. Arthritis Rheum 2002;46:2730–41.
[54] Ogawa N, Kawanami T, Shimoyama K, Ping L, Sugai S. Expression of interferon-inducible T cell chemoattractant (CXCL11) in the salivary glands of patients with Sjogren's syndrome. Clin Immunol 2004;112:235–8.
[55] Hasegawa H, Inoue A, Kohno M, Muraoka M, Miyazaki T, Terada M, et al. Antagonist of interferon-inducible protein 10/CXCL10 ameliorates the progression of autoimmune sialadenitis in MRL/lpr mice. Arthritis Rheum 2006;54:1174–83.

The American Journal of Pathology, Vol. 181, No. 6, December 2012

http://dx.doi.org/10.1016/j.ajpath.2012.08.023

Vascular Biology, Atherosclerosis, and Endothelium Biology

Topical Simvastatin Accelerates Wound Healing in Diabetes by Enhancing Angiogenesis and Lymphangiogenesis

Jun Asai,* Hideya Takenaka,* Satoshi Hirakawa,† Jun-ichi Sakabe,† Asami Hagura,* Saburo Kishimoto,* Kazuichi Maruyama,‡ Kentaro Kajiya,§ Shigeru Kinoshita,‡ Yoshiki Tokura,† and Norito Katoh*

From the Departments of Dermatology and Ophthalmology,‡ Graduate School of Medical Science, Kyoto Prefectural University of Medicine, Kyoto; the Department of Dermatology,† Hamamatsu University School of Medicine, Hamamatsu; and the Shiseido Innovative Science Research Center,§ Yokohama, Japan*

Impaired wound healing is a major complication of diabetes. Recent studies have reported reduced lymphangiogenesis and angiogenesis during diabetic wound healing, which are thought to be new therapeutic targets. Statins have effects beyond cholesterol reduction and can stimulate angiogenesis when used systemically. However, the effects of topically applied statins on wound healing have not been well investigated. The present study tested the hypothesis that topical application of simvastatin would promote lymphangiogenesis and angiogenesis during wound healing in genetically diabetic mice. A full-thickness skin wound was generated on the back of the diabetic mice and treated with simvastatin or vehicle topically. Simvastatin administration resulted in significant acceleration of wound recovery, which was notable for increases in both angiogenesis and lymphangiogenesis. Furthermore, simvastatin promoted infiltration of macrophages, which produced vascular endothelial growth factor C in granulation tissues. *In vitro*, simvastatin directly promoted capillary morphogenesis and exerted an antiapoptotic effect on lymphatic endothelial cells. These results suggest that the favorable effects of simvastatin on lymphangiogenesis are due to both a direct influence on lymphatics and indirect effects via macrophages homing to the wound. In conclusion, a simple strategy of topically applied simvastatin may have significant therapeutic potential for enhanced wound healing in patients with impaired microcirculation such as that in diabetes. *(Am J Pathol 2012, 181:2217–2224; http://dx.doi.org/10.1016/j.ajpath.2012.08.023)*

Delayed wound healing is a major complication of diabetes and is caused by increased apoptosis, delayed cellular infiltration, reduced angiogenesis, and decreased formation and organization of collagen fibers.[1–3] Impaired lymphangiogenesis has also recently been established as a major factor in diabetic refractory wound healing.[4,5] The functions of lymphatic vessels in wounds are to drain the protein-rich lymph from the extracellular space, to maintain normal tissue pressure, and to mediate the immune response.[6,7] Delayed wound healing, such as that seen in infections, appears to result from persistent edema and delayed removal of debris and inflammatory cells due to reduced lymphatic development.[8]

Statins are HMG-CoA (5-hydroxy-3-methylglutaryl-coenzyme A) reductase inhibitors that are primarily used to lower circulating cholesterol levels. In addition, statins have been found to protect against ischemic injury and stimulate angiogenesis in normocholesterolemic animals.[9–11] This angiogenic effect is partially mediated by direct regulation of proliferation of endothelial cells and capillary morphogenesis via the Akt/PI3K pathway.[11] Simvastatin has been found to enhance vascular endothelial growth factor (VEGF) production and improve wound healing in an experimental model of diabetes,[12] and nitropravastatin stimulates reparative neovascularization and improves recovery from limb ischemia in type 1 diabetic mice.[13] However, systemic administration at an extremely high dose was used to obtain angiogenic effects in

Supported by grants from the Ministry of Education, Culture, Sports, Science and Technology of Japan.

Accepted for publication August 15, 2012.

CME Disclosure: The authors of this article and the planning committee members and staff have no relevant financial relationships with commercial interest to disclose.

Supplemental material for this article can be found at *http://ajp.amjapathol.org* or at *http://dx.doi.org/10.1016/j.ajpath.2012.08.023*.

Address reprint requests to Jun Asai, M.D., Ph.D., Department of Dermatology, Graduate School of Medical Science, Kyoto Prefectural University of Medicine, 465 Hirokoji, Kawaramachi, Kamigyo-Ku, Kyoto, 602-8566, Japan. E-mail: jasai@koto.kpu-m.ac.jp.

these studies, and this is inapplicable for clinical use as an angiogenic drug in patients with ischemic disorders. However, topical application of statins with avoidance of systemic adverse effects may be useful for cutaneous wound healing, in which angiogenesis plays a pivotal role.[14] The lymphangiogenic effects of statins have not been widely investigated. In this study, we evaluated the effects of topical simvastatin on angiogenesis and lymphangiogenesis in a mouse model of impaired diabetic wound healing.

Materials and Methods

Animals

Genetically diabetic C57BLKS/J-m+/+*Lepr*^{db} mice (db/db mice) were obtained from Clea Japan, Inc. (Tokyo, Japan). All procedures were performed in accordance with the guidelines of the Animal Care and Use Committees of Kyoto Prefectural University of Medicine.

Creation of Wounds

Mice were between 6 and 10 weeks old at the time of the study. Wounds were generated as described previously.[15–17] In brief, after induction of deep anesthesia by i.p. injection of sodium pentobarbital (160 mg/kg), full-thickness, excisional skin wounds using 8-mm skin biopsy punches were made on the backs of mice, with one wound generated in each mouse. Each wound was covered with a semipermeable polyurethane dressing (OpSite; Smith and Nephew, Massillon, OH) after topical application of simvastatin (Calbiochem, La Jolla, CA) in petroleum jelly (a mixture of 5 mg of simvastatin and 995 mg of jelly) or vehicle (petroleum jelly alone). Simvastatin in petroleum jelly (10 mg of the mixture containing 50 μg of simvastatin) or vehicle were applied to the wound on days 0, 4, 7, and 10 after creation of the wound.

Monitoring of Wound Healing

A total of 5 db/db mice were used at each time point. Wound healing was monitored by taking pictures with a digital camera (Nikon Coolpix 995; Nikon, Tokyo, Japan) on days 0, 4, 7, and 14 after wound creation. Images were analyzed using ImageJ software version 1.46 (NIH, Bethesda, MD)[18] by tracing the wound margin with a high-resolution computer mouse and calculating the pixel area. Wound closure was calculated as follows: Percentage Closed = [(Area on Day 0 − Open Area on Final Day)/Area on Day 0] × 100, as described previously.[15] The areas of the wounds were compared with Student's *t*-test with $P < 0.05$ taken to indicate a significant difference.

Histologic Score

A histologic score was assigned in a masked manner as described previously.[15] Briefly, each specimen received a score of 1 to 12 as follows: 1 to 3, none to minimal cell accumulation and granulation tissue or epithelial migration; 4 to 6, thin, immature granulation dominated by inflammatory cells but with few fibroblasts, capillaries, or collagen deposition and minimal epithelial migration; 7 to 9, moderately thick granulation tissue, ranging from mainly inflammatory cells to more fibroblasts and collagen deposition; and 10 to 12, thick, vascular granulation tissue dominated by fibroblasts and extensive collagen deposition.

Evaluation of Wound Angiogenesis and Lymphangiogenesis

Sections were stained with rat anti-CD31 antibody (1:100) (BD Biosciences, San Jose, CA) or rabbit anti-LYVE-1 antibody (Upstate, Lake Placid, NY). Green fluorescence was generated by labeling with fluorescein isothiocyanate (FITC)–streptavidin (Vector Laboratories, Burlingame, CA) and biotinylated anti-rat or anti-rabbit antibody (both Vector Laboratories). Wound angiogenesis or lymphangiogenesis was analyzed by calculating the percentage of fluorescent area.[16,19] Briefly, for each slide, an image of the granulation tissue at the wound margin was captured. ImageJ software was used to quantitate the fluorescence intensity. The mean percentage of fluorescent pixels of five images served as an index of the angiogenic or lymphangiogenic response.

Evaluation of Macrophage Number, Phenotype, and VEGF-C Expression in Granulation Tissue

Sections of wounds were stained with rat anti-F4/80 antibody (Invitrogen, Carlsbad, CA). Labeling with F4/80 was visualized with Cy3-conjugated anti-rat antibody (Vector Laboratories). Ten granulation tissue fields (two sections from each animal) were selected, and F4/80-positive cells were counted.[16] VEGF-C expression was evaluated using goat anti-VEGF-C antibody (Santa Cruz Biotechnology, Santa Cruz, CA) and FITC-conjugated anti-goat antibody (Vector Laboratories). To determine the phenotype of infiltrating macrophages, IL-13 and tumor necrosis factor (TNF) α expression was evaluated using goat anti-IL-13 antibody and goat anti-TNF-α antibody (Santa Cruz Biotechnology), respectively, and FITC-conjugated anti-goat antibody. F4/80-positive TNF-α–positive cells were defined as an M1 phenotype and F4/80-positive IL-13–positive cells as an M2 phenotype. In each slide, F4/80-positive cells, F4/80-positive TNF-α–positive cells, and F4/80-positive IL-13–positive cells were counted, and percentages of TNF-α–positive macrophages and IL-13–positive macrophages were evaluated. The mean percentages of TNF-α–positive macrophages and IL-13–positive macrophages in five images were used as indexes of the M1 and M2 phenotypes, respectively.

RNA Isolation, cDNA Synthesis, and Quantitative RT-PCR

Tissue sections obtained in RNAlater (Ambion, Paisley, UK) were processed for RNA isolation, cDNA synthesis, and quantitative RT-PCR.[16] VEGF-C, fibroblast growth factor 2, endothelial nitric oxide synthase, stromal cell-derived factor 1α, and platelet-derived growth factor β gene expression levels were normalized based on the level of an internal

reference gene, 18S. The primers used in the study were obtained from QIAGEN (Dűsseldorf, Germany).

Cell Culture

Primary human lymphatic endothelial cells (LECs) were collected as previously described.[20] LECs were cultured at 37°C in 5% CO_2 in endothelial cell basal medium 2 (Lonza, Walkersville, MD) supplemented with 5% fetal bovine serum, human VEGF-A, human fibroblast growth factor 2, human epidermal growth factor, insulin-like growth factor 1, and ascorbic acid. Each experiment was conducted at least three times, with similar results. A representative experiment is shown.

Western Blot Analysis

Cells were lysed with RIPA buffer (Invitrogen) and sonicated. After sonication, cell lysates were centrifuged at 15,400 × *g* for 20 minutes at 4°C, and the supernatants were collected into fresh tubes. Then 4× SDS sample buffer with 0.1 mol/L dithiothreitol was added to samples. Samples were boiled for 5 minutes at 95°C, and 20-μg extracts were separated by 10% SDS-PAGE and electroblotted onto polyvinylidene difluoride membranes for 2 hours at 180 mA. The membranes were incubated with rabbit anti-human Akt (pan) (C67E7) monoclonal antibody (Cell Signaling Technology, Danvers, MA), rabbit anti-human phospho-Akt (Ser473) (D9E) monoclonal antibody (Cell Signaling Technology), or mouse anti-GAPDH monoclonal antibody (Santa Cruz Biotechnology) and detected with horseradish peroxidase–conjugated goat anti-rabbit IgG (Bio-Rad, Hercules, CA) or horseradish peroxidase–conjugated goat anti-mouse IgG (Bio-Rad). Immunoblots were visualized using an ECL Plus Western Blotting Detection Reagents Kit (GE Healthcare, Little Chalfont, Buckinghamshire, UK) according to the manufacturer protocol.

Chord Formation Assay

LECs were used in a chord formation assay.[21] An aliquot (100 μL) of growth factor–depleted Matrigel (Becton Dickinson, Bedford, MA) was added to a 24-well dish and allowed to gel for 30 minutes at 37°C. LECs were seeded at 5×10^4 cells/mL in 500 μL of endothelial cell basal medium 2 containing 3% fetal bovine serum. Cells were cultured in the absence or presence of various doses of simvastatin (Calbiochem, Darmstadt, Germany) with or without pretreatment with a PI3 kinase inhibitor, LY294002 (50 μmol/L) (ENZO Life Sciences, Plymouth Meeting, PA), the mTOR/raptor inhibitor rapamycin (100 nmol/L) (Merck Millipore, Darmstadt, Germany), or the PI3K/mTOR inhibitor wortmannin-rapamycin (100 nmol/L) (Cayman Chemical, Ann Arbor, MI) for 30 minutes. Chord formation was monitored for 24 hours. Digital pictures were taken using a spot image analysis system, and the total length of the chord-like structures at 12 hours was outlined and measured using ImageJ software.

Proliferation Assay

The proliferative activity of cells treated with simvastatin was examined using a CellTiter 96 nonradioactive cell proliferation assay (Promega, Madison, WI). Briefly, subconfluent cells (5000 cells per well) were reseeded on 96-well, flat-bottomed plates with 100 μL of growth media. The cells were treated with simvastatin and incubated for 48 hours at 37°C. Absorbance at 570 nm was recorded using a 96-well enzyme-linked immunosorbent assay (ELISA) plate reader.

Apoptosis Assay

An apoptosis assay was performed using a DeadEnd Fluorometric TUNEL System (Promega). Briefly, LECs were plated on chamber slides and placed in medium. Cells were stimulated by simvastatin and incubated for 24 hours with medium containing 400 μmol/L H_2O_2. To quantify apoptosis, 400 nuclei from random microscopic fields were analyzed by an observer masked to the treatment groups. The number of apoptotic cells was expressed as a percentage of the total cell count.

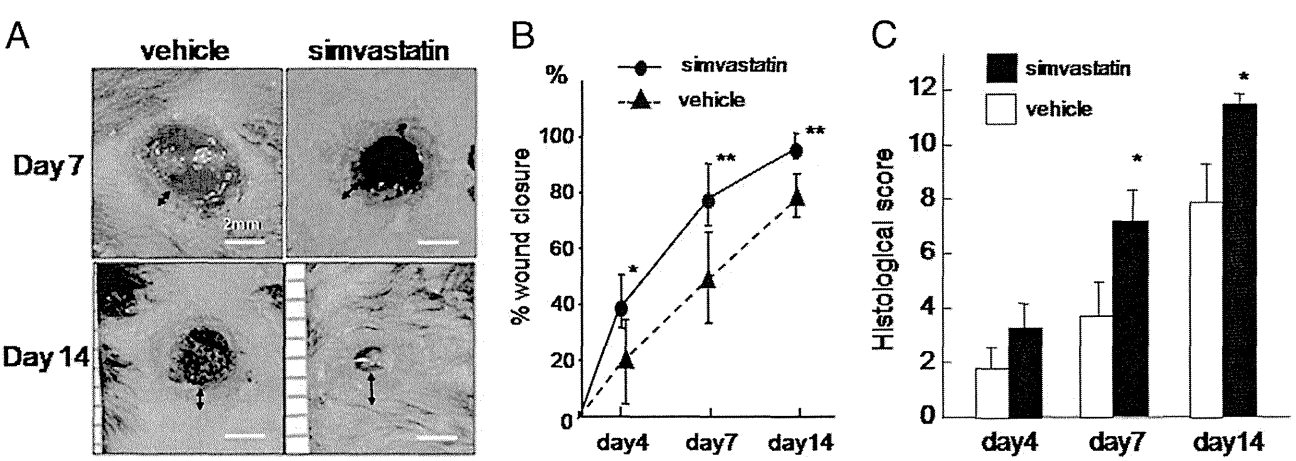

Figure 1. Effects of topical simvastatin on wound closure and histologic score in db/db mice. **A:** Representative macroscopic views of wounds after different treatments and periods. Scale bar = 2 mm. **Arrows** indicate the epithelialized range. **B:** Wound closure was measured on days 4, 7, and 14. $^*P < 0.05$, $^{**}P < 0.001$ versus vehicle ($n = 5$ in each group). **C:** Histologic scores for days 4, 7, and 14, quantified as described in *Materials and Methods*. Higher histologic scores indicate a greater extent of wound healing. $^*P < 0.05$ versus vehicle ($n = 5$ in each group).

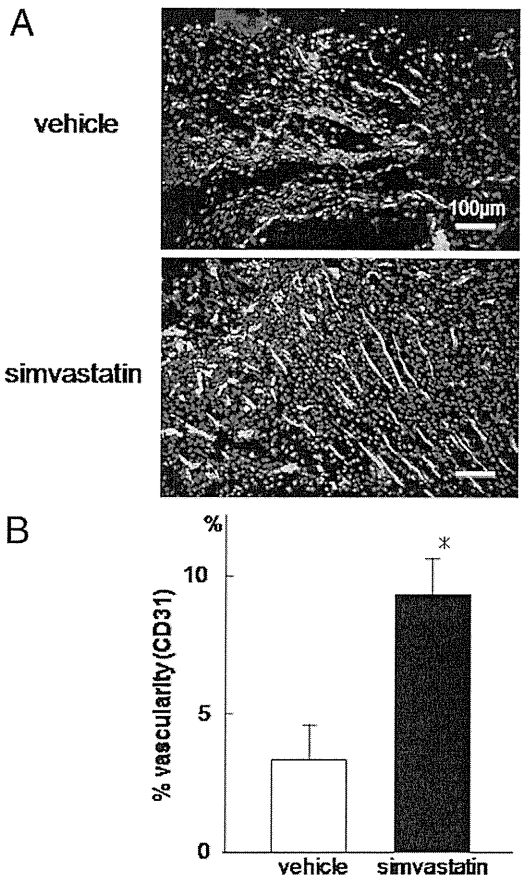

Figure 2. Effects of simvastatin on vascularity in granulation tissues at the wound margin in db/db mice. **A:** Neovascularization at the wound margin in simvastatin- or vehicle-treated diabetic mice after 14 days. Original magnification, ×100. Scale bar = 100 μm. Green and blue fluorescence corresponds to CD31-positive newly formed blood vessels and DAPI-labeled nuclei, respectively. **B:** Percentage of vascularity, quantified as described in *Materials and Methods*. *$P < 0.001$ versus vehicle ($n = 5$ in each group).

Statistical Analysis

All results are presented as mean ± SEM. Statistical comparisons between two groups were performed by Student's *t*-test. Multiple groups were analyzed by one-way analysis of variance followed by appropriate post hoc tests to determine statistical significance. $P < 0.05$ was considered significant. All *in vitro* experiments were performed at least in triplicate.

Results

Simvastatin Accelerates Wound Healing in Diabetic Mice

Wound areas on days 7 and 14 in simvastatin- or vehicle-treated diabetic mice are shown in Figure 1A. On day 14, simvastatin-treated wounds had more than 90% epithelialization, whereas <80% of the wound was epithelialized in the vehicle-treated group (Figure 1B). Simvastatin treatment resulted in significantly smaller wound areas after 4, 7, and 14 days. The difference in percentage of wound closure reached a maximum on day 7 (simvastatin versus control: 79.26% ± 11.09% versus 52.45% ± 16.81%; $P < 0.001$). The histologic score reflects the degree of maturation of granulation tissue, including inflammation, collagen deposition, and reepithelialization, in addition to neovascularization; therefore, higher histologic scores reflect a greater extent of wound healing. The histologic scores for wounds treated with simvastatin were significantly higher than those in the vehicle-treated group (day 4: 3.6 ± 0.70 versus 1.9 ± 0.73; day 7: 7.3 ± 0.94 versus 3.7 ± 0.94, $P < 0.01$; day 14: 11.6 ± 0.51 versus 8.0 ± 1.15, $P < 0.01$)(Figure 1C).

Simvastatin Promotes Both Angiogenesis and Lymphangiogenesis

Wound angiogenesis was analyzed by immunostaining of an endothelial cell–specific marker, CD31, in 10-μm frozen sections to visualize neovascularization. Figure 2A shows neovascularization at the margin in simvastatin- or vehicle-treated wounds in diabetic mice on day 14. A few small vessels were seen at the wound margin in the vehicle-treated group, whereas large numbers of vessels were growing toward the center of the wound in the

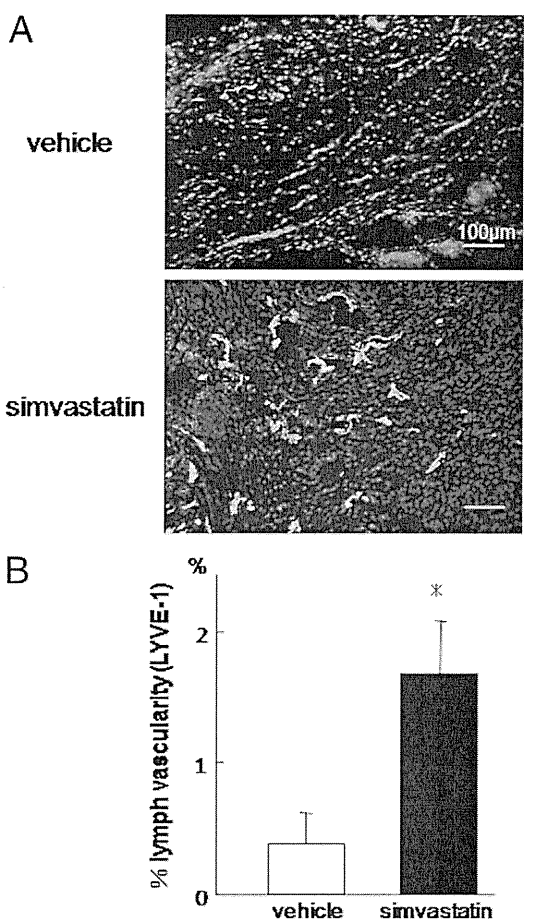

Figure 3. Effects of simvastatin on lymphangiogenesis in granulation tissues at the wound margin in db/db mice. **A:** Lymphangiogenesis at the wound margin in simvastatin- or vehicle-treated diabetic mice after 14 days. Original magnification, ×100. Scale bar =100 μm. Green and blue fluorescence corresponds to LYVE-1–positive newly formed lymphatic vessels and DAPI-labeled nuclei, respectively. **B:** Percentage of lymphatic vascularity, quantified as described in *Materials and Methods*. *$P < 0.001$ versus vehicle ($n = 5$ in each group).

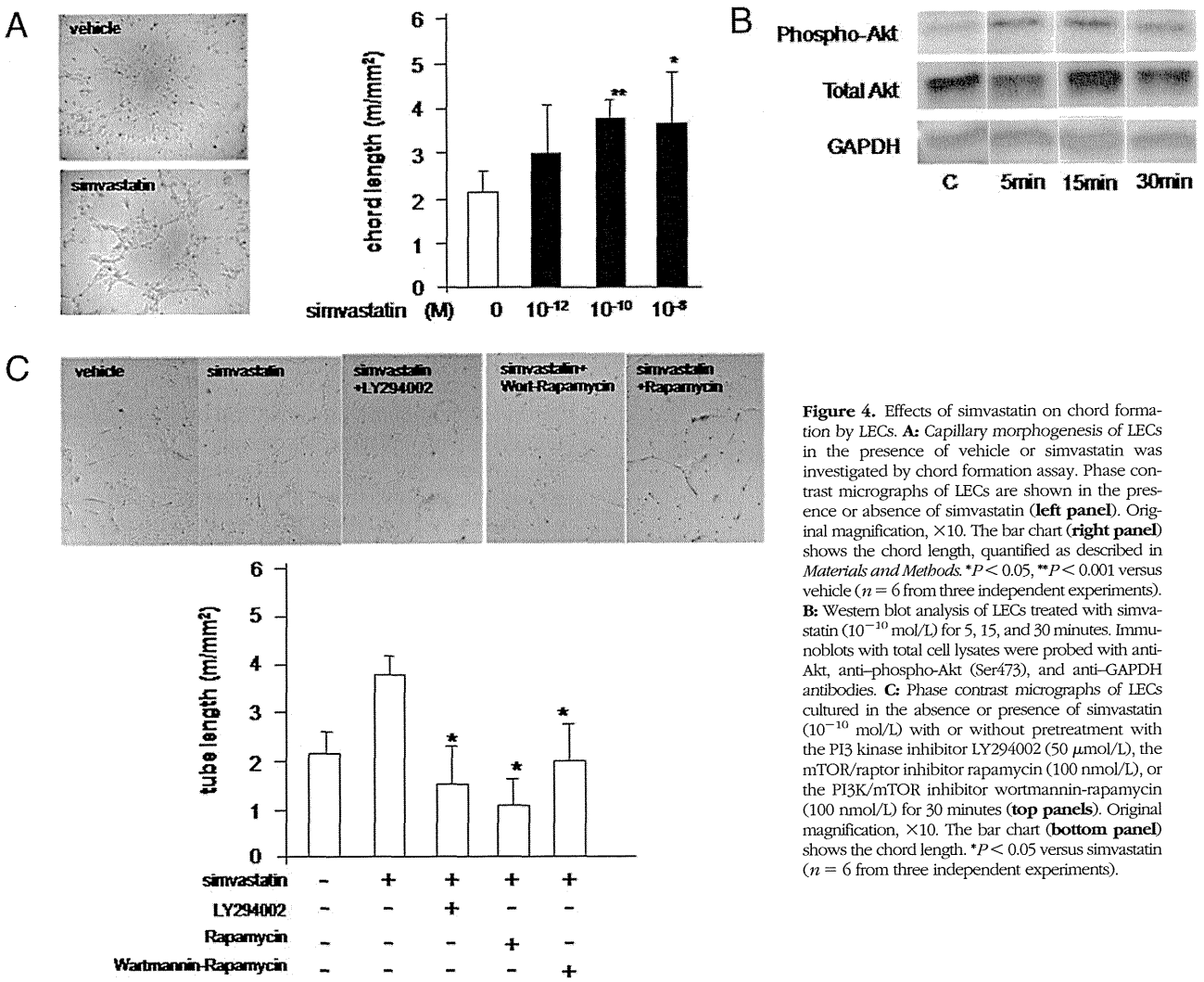

Figure 4. Effects of simvastatin on chord formation by LECs. **A:** Capillary morphogenesis of LECs in the presence of vehicle or simvastatin was investigated by chord formation assay. Phase contrast micrographs of LECs are shown in the presence or absence of simvastatin (**left panel**). Original magnification, ×10. The bar chart (**right panel**) shows the chord length, quantified as described in *Materials and Methods*. $^{*}P < 0.05$, $^{**}P < 0.001$ versus vehicle ($n = 6$ from three independent experiments). **B:** Western blot analysis of LECs treated with simvastatin (10^{-10} mol/L) for 5, 15, and 30 minutes. Immunoblots with total cell lysates were probed with anti-Akt, anti–phospho-Akt (Ser473), and anti-GAPDH antibodies. **C:** Phase contrast micrographs of LECs cultured in the absence or presence of simvastatin (10^{-10} mol/L) with or without pretreatment with the PI3 kinase inhibitor LY294002 (50 μmol/L), the mTOR/raptor inhibitor rapamycin (100 nmol/L), or the PI3K/mTOR inhibitor wortmannin-rapamycin (100 nmol/L) for 30 minutes (**top panels**). Original magnification, ×10. The bar chart (**bottom panel**) shows the chord length. $^{*}P < 0.05$ versus simvastatin ($n = 6$ from three independent experiments).

simvastatin group. Simvastatin significantly enhanced wound vascularity based on image analysis of the percentage of the fluorescent area (9.29% ± 1.29% versus 3.25% ± 1.33%; $P < 0.001$)(Figure 2B). Wound lymphangiogenesis was analyzed by immunostaining of a LEC-specific marker, LYVE-1, in 10-μm frozen sections. Figure 3A shows new lymphatic vessels at the margin of simvastatin- or vehicle-treated wounds in diabetic mice on day 14. Wound lymphatic vascularity was significantly enhanced by simvastatin (percentage of fluorescent area: 1.72% ± 0.460% versus 0.395% ± 0.260%; $P < 0.001$) (Figure 3B). New vessels and lymphatics in granulation tissue in both groups were not covered with α-smooth muscle actin–positive mural cells (see Supplemental Figure S1 at *http://ajp.amjpathol.org*).

Simvastatin Induces Capillary Morphogenesis of LECs and Has an Antiapoptotic Effect but Does Not Induce Proliferation

To characterize the effects of simvastatin on lymphangiogenesis, we performed a chord formation assay in primary human LECs *in vitro*. Treatment with simvastatin promoted LEC chord formation in a dose-dependent manner (Figure 4A). This effect was significantly blocked by the PI3 kinase inhibitor LY294002, the mTOR inhibitor rapamycin, and the PI3/mTOR inhibitor wortmannin-rapamycin ($P < 0.05$)(Figure 4C). The proliferative and antiapoptotic effects of simvastatin on LECs were also examined because these are major effects of simvastatin in vascular endothelial cells. Simvastatin did not promote LEC proliferation, even at higher concentrations, and seemed to be slightly cytotoxic at 10^{-6} mol/L and 10^{-5} mol/L (Figure 5A). However, simvastatin treatment resulted in significant inhibition of H_2O_2-induced apoptosis compared with controls (Figure 5B).

Simvastatin Promotes Macrophage Infiltration and VEGF-C Production in Wounds

The number of macrophages in granulation tissues was evaluated in wounds on day 7. This timing was chosen because reepithelialization was almost complete on day 14 in simvastatin-treated wounds, and inflammatory cells had already diminished. The number of macrophages in simvastatin-treated wounds on day 7 was significantly

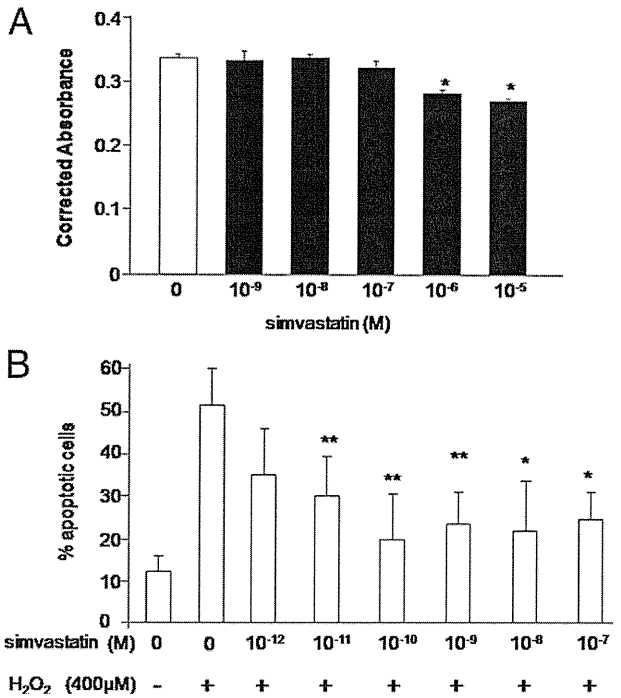

Figure 5. Effects of simvastatin on proliferation and apoptosis of LECs. **A:** Cell proliferation of LECs was investigated by MTS assay. Subconfluent cells (5000 cells per well) were reseeded on 96-well, flat-bottomed plates with 100 μL of growth media. The cells were treated with simvastatin and incubated for 48 hours at 37°C. Absorbance at 570 nm was recorded using a 96-well ELSIA plate reader. Quantification was performed as described in *Materials and Methods*. $^*P < 0.05$ versus vehicle ($n = 8$ from three independent experiments). **B:** Cell apoptosis in LECs was investigated by TUNEL assay. LECs were plated on chamber slides and placed in medium. Cells were stimulated by simvastatin and incubated for 24 hours with medium containing 400 μmol/L H_2O_2. Quantification of apoptotic cells was performed as described in *Materials and Methods*. $^*P < 0.05$, $^{**}P < 0.01$ versus H_2O_2 treatment ($n = 3$ from three independent experiments).

greater than that in controls (Figure 6, A and B). Most of the macrophages in the simvastatin-treated group expressed the M2 marker, IL-13, rather than the M1 marker, TNF-α, whereas most macrophages in the vehicle-treated group expressed TNF-α rather than IL-13 (Figure 6, C–F). The macrophages in the simvastatin-treated group produced VEGF-C (Figure 7A), and VEGF-C expression was significantly up-regulated in simvastatin-treated wounds compared with controls (Figure 7B). Other proangiogenic mediators in wound granulation tissue were evaluated by real-time PCR. Platelet-derived growth factor β, endothelial nitric oxide synthase, and fibroblast growth factor 2 were significantly up-regulated by simvastatin stimulation (see Supplemental Figure S2 at *http://ajp.amjpathol.org*).

Discussion

In this study, we found that topical application of simvastatin accelerated diabetic wound healing via promotion of angiogenesis and lymphangiogenesis. Many studies have reported that statins, including simvastatin, have strong angiogenic effects on vascular endothelial cells or placental stem cells and that these effects are mainly mediated by the PI3-kinase/Akt pathway,[11,22,23] although we note that other findings have also been reported[24] Consistent with these reports, abundant neovascularization and proangiogenic growth factors were observed in wounds treated with topical simvastatin in our *in vivo* study. Statins were originally introduced as systemic antihyperlipidemic drugs; however, a recent study has shown the value of topical simvastatin.[14] An advantage of topical application is that a suitable concentration of simvastatin can be applied without a risk of serious systemic adverse effects, such as rhabdomyolysis. Our results suggest that topical application of simvastatin could be a

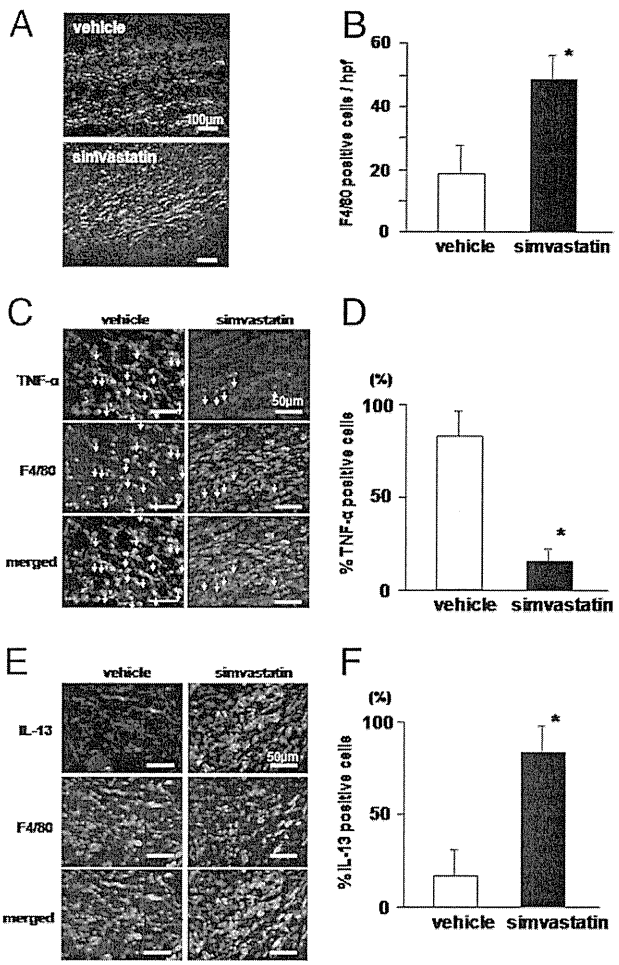

Figure 6. Effects of simvastatin on macrophage infiltration and phenotype in granulation tissue. **A:** Representative photomicrographs of the immunostained wound edge at 7 days after wound creation. Red fluorescence corresponds to F4/80-positive macrophages. Scale bar = 100 μm. **B:** The macrophage count, quantified as described in *Materials and Methods*. $^*P < 0.05$ versus vehicle ($n = 5$). **C:** Representative photomicrographs of the immunodetection of TNF-α and F4/80 in histologic sections from vehicle- or simvastatin-treated wounds (original magnification ×400). Scale bar = 50 μm. Green and red fluorescence corresponds to TNF-α–positive cells and F4/80-positive macrophages, respectively. Yellow indicates TNF-α–producing M1 phenotype macrophages (**white arrows**). **D:** Quantification of percentage of TNF-α–positive macrophages, as described in *Materials and Methods*. $^*P < 0.001$ versus vehicle ($n = 5$ in each group). **E:** Representative photomicrographs of immunodetection of IL-13 and F4/80 in histologic sections from vehicle- or simvastatin-treated wounds (original magnification ×400). Scale bar = 50 μm. Green and red fluorescence correspond to IL-13–positive cells and F4/80-positive macrophages, respectively. Yellow indicates IL-13–producing M2 phenotype macrophages. **F:** Quantification of percentage of IL-13–positive macrophages, as described in *Materials and Methods*. $^*P < 0.001$ versus vehicle ($n = 5$ in each group).

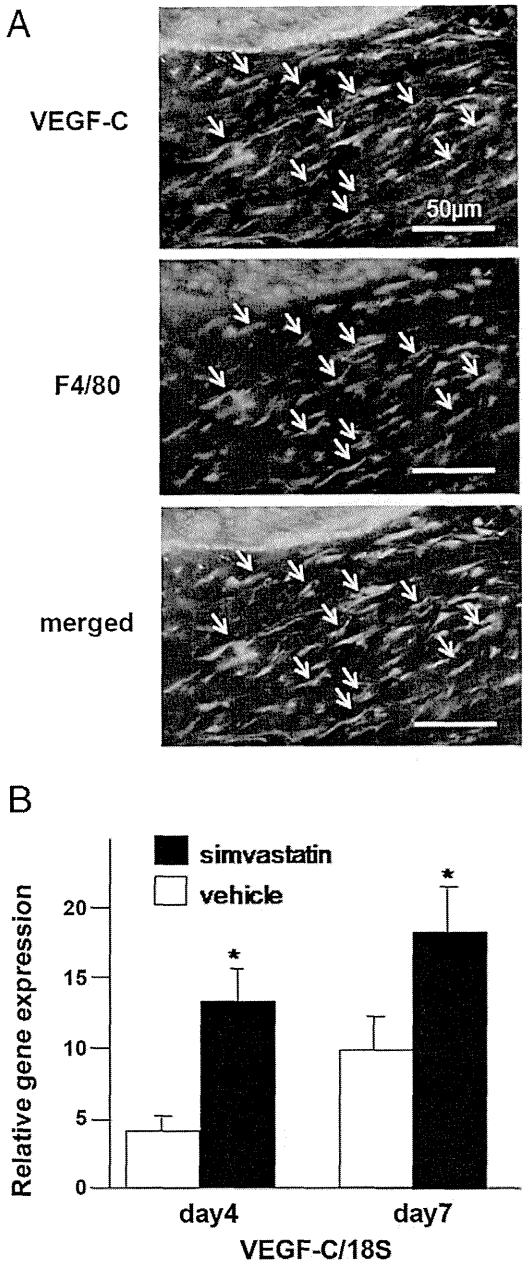

Figure 7. VEGF-C expression in granulation tissue. **A:** Representative photomicrographs of the immunostained wound edge treated with simvastatin at 7 days after wound creation. Green and red fluorescence indicates VEGF-C expression and F4/80-positive macrophages, respectively. Original magnification, ×400. **Arrows** indicate double-positive cells. Scale bar = 50 μm. **B:** Quantitative RT-PCR of VEGF-C in wound granulation tissue. Gene expression levels were normalized based on the level of an internal reference gene, 18S. $^*P < 0.05$ versus vehicle ($n = 5$).

new therapeutic strategy for treatment of local ischemic conditions, such as those in patients with diabetic ulcers.

Lymphangiogenesis is a major factor in diabetic refractory wound healing.[4,5] Therefore, we focused on the effects of simvastatin on wound lymphangiogenesis. Recent studies have suggested that several biological functions of LECs are partially regulated by the AKT/PI3K/mTOR pathway.[25,26] Consistent with these observations, capillary morphogenesis of LECs was significantly stimulated by simvastatin as an effect on vascular endothelial cells that was, at least in part, regulated by the AKT/PI3K/mTOR pathway. Our results suggest that the mechanisms underlying the lymphangiogenic effects of simvastatin in LECs might be similar to those for angiogenic effects. These mechanisms include antiapoptosis and promotion of capillary morphogenesis because LECs develop from a vascular network in an embryonic stage,[27] and these cells have a similar lineage. However, contrary to our expectation, simvastatin did not promote proliferation of LECs *in vitro*. During the wound healing process, new lymphatics are formed in newly generated granulation tissue, indicating that proliferation of preexisting lymphatic vessels is needed.

Because simvastatin did not promote the proliferation of LECs, we evaluated other possible sources of lymphangiogenic factors. Several reports suggest that infiltrating macrophages contribute to lymphangiogenesis as the major producer of VEGF-C in cutaneous wound healing,[4,5] and therefore we evaluated the effects of simvastatin on macrophages. Macrophages carry VEGF receptor 3, in addition to producing VEGF-C, and thus act as both autocrine and paracrine factors. We have previously reported that healing impairment in diabetes involves reduced lymphangiogenesis and suppressed macrophage function, such as recruitment to inflammatory sites and secretion of growth factors.[5] In this study, the number of infiltrating macrophages in granulation tissue was significantly increased by topical application of simvastatin, and most of these macrophages produced VEGF-C. These observations suggest that simvastatin recovers lymphangiogenic function that is impaired in macrophages under diabetic conditions.

Increased apoptosis is a major concern in wound healing in a diabetic state.[3,28–31] Hyperglycemia induces proinflammatory cytokines, such as TNF-α, and oxidative stress, which result in increased apoptosis in diabetes. Our study found that most infiltrating macrophages in diabetic wounds had an M1 proinflammatory phenotype producing abundant TNF-α. Simvastatin decreased H_2O_2-induced apoptosis in LECs *in vitro* and increased M2 anti-inflammatory phenotype macrophages in granulation tissue *in vivo*. We suggest that this anti-apoptotic effect of simvastatin also plays an important role, in addition to promotion of angiogenesis and lymphangiogenesis.

Increased infiltration of macrophages induced by simvastatin may have further benefits because the histologic scores of diabetic wounds were significantly improved by topical application of simvastatin. The histologic score reflects the degree of maturation of granulation tissue, including inflammation, collagen deposition, and reepithelialization, in addition to neovascularization. Macrophages play a central role in all stages of wound healing and orchestrate the wound healing process[32] by exerting proinflammatory functions and facilitating wound healing during the early stage and stimulating proliferation of fibroblasts, keratinocytes, and endothelial cells in the proliferative stage. Because the main focus of this study was lymphangiogenesis, we did not investigate the effects of simvastatin on reepithelialization or formation of extracellular matrix. This will require further experiments in a future study.

In conclusion, regulation of apoptosis and capillary differentiation are essential for development of functional lymphatics during wound healing. The findings of the present study suggest that topical simvastatin can stimulate lymp-

hangiogenesis directly and indirectly via stimulation of macrophages. Vascular remodeling induced by simvastatin might have therapeutic potential in patients with microvascular dysfunction, such as that in diabetic foot ulcer, a major cause of morbidity in the growing population of patients with diabetes. A future investigation is warranted to determine the potential clinical utility of this approach.

References

1. Jeffcoate WJ, Harding KG: Diabetic foot ulcers. Lancet 2003, 361: 1545–1551
2. Lerman OZ, Galiano RD, Armour M, Levine JP, Gurtner GC: Cellular dysfunction in the diabetic fibroblast: impairment in migration, vascular endothelial growth factor production, and response to hypoxia. Am J Pathol 2003, 162:303–312
3. Fadini GP, Albiero M, Menegazzo L, Boscaro E, Pagnin E, Iori E, Cosma C, Lapolla A, Pengo V, Stendardo M, Agostini C, Pelicci PG, Giorgio M, Avogaro A: The redox enzyme p66Shc contributes to diabetes and ischemia-induced delay in cutaneous wound healing. Diabetes 2010, 59:2306–2314
4. Saaristo A, Tammela T, Farkkila A, Karkkainen M, Suominen E, Yla-Herttuala S, Alitalo K: Vascular endothelial growth factor-C accelerates diabetic wound healing. Am J Pathol 2006, 169:1080–1087
5. Maruyama K, Asai J, Ii M, Thorne T, Losordo DW, D'Amore PA: Decreased macrophage number and activation lead to reduced lymphatic vessel formation and contribute to impaired diabetic wound healing. Am J Pathol 2007, 170:1178–1191
6. Oliver G, Detmar M: The rediscovery of the lymphatic system: old and new insights into the development and biological function of the lymphatic vasculature. Genes Dev 2002, 16:773–783
7. Witte MH, Bernas MJ, Martin CP, Witte CL: Lymphangiogenesis and lymphangiodysplasia: from molecular to clinical lymphology. Microsc Res Tech 2001, 55:122–145
8. Ji RC: Characteristics of lymphatic endothelial cells in physiological and pathological conditions. Histol Histopathol 2005, 20:155–175
9. Werner N, Nickenig G, Laufs U: Pleiotropic effects of HMG-CoA reductase inhibitors. Basic Res Cardiol 2002, 97:105–116
10. Landmesser U, Engberding N, Bahlmann FH, Schaefer A, Wiencke A, Heineke A, Spiekermann S, Hilfiker-Kleiner D, Templin C, Kotlarz D, Mueller M, Fuchs M, Hornig B, Haller H, Drexler H: Statin-induced improvement of endothelial progenitor cell mobilization, myocardial neovascularization, left ventricular function, and survival after experimental myocardial infarction requires endothelial nitric oxide synthase. Circulation 2004, 110:1933–1939
11. Kureishi Y, Luo Z, Shiojima I, Bialik A, Fulton D, Lefer DJ, Sessa WC, Walsh K: The HMG-CoA reductase inhibitor simvastatin activates the protein kinase Akt and promotes angiogenesis in normocholesterolemic animals. Nat Med 2000, 6:1004–1010
12. Bitto A, Minutoli L, Altavilla D, Polito F, Fiumara T, Marini H, Galeano M, Calo M, Lo Cascio P, Bonaiuto M, Migliorato A, Caputi AP, Squadrito F: Simvastatin enhances VEGF production and ameliorates impaired wound healing in experimental diabetes. Pharmacol Res 2008, 57:159–169
13. Emanueli C, Monopoli A, Kraenkel N, Meloni M, Gadau S, Campesi I, Ongini E, Madeddu P: Nitropravastatin stimulates reparative neovascularisation and improves recovery from limb ischaemia in type-1 diabetic mice. Br J Pharmacol 2007, 150:873–882
14. Otuki MF, Pietrovski EF, Cabrini DA: Topical simvastatin: preclinical evidence for a treatment of skin inflammatory conditions. J Dermatol Sci 2006, 44:45–47
15. Greenhalgh DG, Sprugel KH, Murray MJ, Ross R: PDGF and FGF stimulate wound healing in the genetically diabetic mouse. Am J Pathol 1990, 136:1235–1246
16. Asai J, Takenaka H, Katoh N, Kishimoto S: Dibutyryl cAMP influences endothelial progenitor cell recruitment during wound neovascularization. J Invest Dermatol 2006, 126:1159–1167
17. Asai J, Takenaka H, Kusano KF, Ii M, Luedemann C, Curry C, Eaton E, Iwakura A, Tsutsumi Y, Hamada H, Kishimoto S, Thorne T, Kishore R, Losordo DW: Topical sonic hedgehog gene therapy accelerates wound healing in diabetes by enhancing endothelial progenitor cell-mediated microvascular remodeling. Circulation 2006, 113:2413–2424
18. Abràmoff MD, Magalhães PJ, Ram S: J: image processing with ImageJ. Biophotonics Int 2004, 11:36–42
19. Jacobi J, Jang JJ, Sundram U, Dayoub H, Fajardo LF, Cooke JP: Nicotine accelerates angiogenesis and wound healing in genetically diabetic mice. Am J Pathol 2002, 161:97–104
20. Hirakawa S, Hong YK, Harvey N, Schacht V, Matsuda K, Libermann T, Detmar M: Identification of vascular lineage-specific genes by transcriptional profiling of isolated blood vascular and lymphatic endothelial cells. Am J Pathol 2003, 162:575–586
21. Maruyama K, Ii M, Cursiefen C, Jackson DG, Keino H, Tomita M, Van Rooijen N, Takenaka H, D'Amore PA, Stein-Streilein J, Losordo DW, Streilein JW: Inflammation-induced lymphangiogenesis in the cornea arises from CD11b-positive macrophages. J Clin Invest 2005, 115:2363–2372
22. Nakao T, Shiota M, Tatemoto Y, Izumi Y, Iwao H: Pravastatin induces rat aortic endothelial cell proliferation and migration via activation of PI3K/Akt/mTOR/p70 S6 kinase signaling. J Pharmacol Sci 2007, 105:334–341
23. Cantoni S, Cavallini C, Bianchi F, Bonavita F, Vaccari V, Olivi E, Frascari I, Tassinari R, Valente S, Lionetti V, Ventura C: Rosuvastatin elicits KDR-dependent vasculogenic response of human placental stem cells through PI3K/AKT pathway. Pharmacol Res 2012, 65:275–284
24. Zhao TT, Trinh D, Addison CL, Dimitroulakos J: Lovastatin inhibits VEGFR and AKT activation: synergistic cytotoxicity in combination with VEGFR inhibitors. PLoS One 2010, 5:e12563
25. Luo Y, Liu L, Rogers D, Su W, Odaka Y, Zhou H, Chen W, Shen T, Alexander JS, Huang S: Rapamycin inhibits lymphatic endothelial cell tube formation by downregulating vascular endothelial growth factor receptor 3 protein expression. Neoplasia 2012, 14:228–237
26. Dellinger MT, Brekken RA: Phosphorylation of Akt and ERK1/2 is required for VEGF-A/VEGFR2-induced proliferation and migration of lymphatic endothelium. PLoS One 2011, 6:e28947
27. Oliver G: Lymphatic vasculature development. Nat Rev Immunol 2004, 4:35–45
28. Hamed S, Ullmann Y, Egozi D, Daod E, Hellou E, Ashkar M, Gilhar A, Teot L: Fibronectin potentiates topical erythropoietin-induced wound repair in diabetic mice. J Invest Dermatol 2011, 131:1365–1374
29. Badr G: Supplementation with undenatured whey protein during diabetes mellitus improves the healing and closure of diabetic wounds through the rescue of functional long-lived wound macrophages. Cell Physiol Biochem 2012, 29:571–582
30. Ahmad J, Zubair M, Malik A, Siddiqui MA, Wangnoo SK: Cathepsin-D, Adiponectin, TNF-alpha, IL-6 and hsCRP plasma levels in subjects with diabetic foot and possible correlation with clinical variables: a multicentric study. Foot (Edinb) 2012, 22:194–199
31. Dave GS, Kalia K: Hyperglycemia induced oxidative stress in type-1 and type-2 diabetic patients with and without nephropathy. Cell Mol Biol (Noisy-le-grand) 2007, 53:68–78
32. Mahdavian Delavary B, van der Veer WM, van Egmond M, Niessen FB, Beelen RH: Macrophages in skin injury and repair. Immunobiology 2011, 216:753–762

Journal of Photochemistry and Photobiology B: Biology 113 (2012) 56–62

Contents lists available at SciVerse ScienceDirect

Journal of Photochemistry and Photobiology B: Biology

journal homepage: www.elsevier.com/locate/jphotobiol

Addition of UVA-absorber butyl methoxy dibenzoylmethane to topical ketoprofen formulation reduces ketoprofen-photoallergic reaction

Kenji Atarashi [a,*], Masashi Takano [a], Shunsuke Kato [a], Hidekazu Kuma [a], Masaru Nakanishi [a], Yoshiki Tokura [b]

[a] Basic Research Laboratories, R&D Division, Hisamitsu Pharmaceutical Co., Inc., 1-25-11, Kannondai, Tsukuba 305-0856, Japan
[b] Department of Dermatology, Hamamatsu University School of Medicine, 1-20-1, Handayama, Higashi-ku, Hamamatsu 431-3192, Japan

ARTICLE INFO

Article history:
Received 17 January 2012
Received in revised form 27 March 2012
Accepted 3 May 2012
Available online 17 May 2012

Keywords:
Ketoprofen
Butyl methoxy dibenzoylmethane
UVA
Photoallergy
Photocontact dermatitis
Plaster

ABSTRACT

Topical application of ketoprofen (KP) clinically evokes the allergic type of photocontact dermatitis. To avoid this adverse reaction, we investigated the beneficial effect of each ultraviolet (UV) filter that was included in topical ketoprofen formulation. We first tested the inhibitory effects of four UVA filters by a modified local lymph node assay following KP application on the mouse skin and UVA irradiation on the same site. In this assessment, butyl methoxy dibenzoylmethane (BMDBM), when included in KP application, exerted the most effective inhibitory effect on stimulation with KP and UVA. We manufactured topical patch and gel KP applicants containing BMDBM, which retained KP penetration through the skin and KP stability toward UVA. The ability of BMDBM in these formulations to inhibit KP photosensitivity was evaluated by a modified adjuvant and strip method in guinea pigs, and the photoallergic reactions induced by the BMDBM-containing KP applicants were lower than the non-containing ones. It is known that KP has a cross-reactivity with benzophenone upon UVA exposure, but such a photocross-reactivity of BMDBM with KP was not observed in a mouse ear swelling model. The anti-inflammatory effect of the BMDBM-containing KP patch applicant was comparable to the non-containing one. These results suggest that the addition of BMDBM into KP topical formulations is efficacious for inhibition of KP photocontact dermatitis.

1. Introduction

Various topical agents, such as antibacterial agents, perfumes, sunscreens, and non-steroidal anti-inflammatory drugs (NSAIDs), have been reported to cause photocontact dermatitis [1]. This sensitivity is evoked when these agents are topically applied to the skin and the same site was subsequently exposed to ultraviolet (UV) light. The photoreactions are divided into the phototoxic and photoallergic types. While the phototoxic reaction is mediated by oxygen intermediates without specific immune reactions [2,3], photoallergic reaction occurs as a consequence of a specific immune reaction mediated by antigen-specific, sensitized T cells [4–8]. Two mechanisms have been put forward in T-cell recognition of photoallergic small molecules as photoantigen, i.e. photohapten and prohapten theories [1,5,8]. According to the photohapten theory, photosensitizing chemicals and protein need to coexist, and upon exposure to UV, the chemicals bind covalently to protein. On the other hand, the prohapten theory suggests that UV simply converts photosensitizing substances into ordinary hapten, which subsequently binds to protein.

Ketoprofen (KP) is widely used as a topical NSAID, since its transdermal penetration and pharmacological efficiency are superior to other NSAIDs such as diclofenac and indomethacin [9]. Whereas orally administered NSAIDs may cause gastrointestinal and cardiovascular adverse reactions, the skin application of NSAIDs very rarely induces these systemic side effects. However, topical formulations of KP may provoke photocontact dermatitis as an adverse reaction. KP has both phototoxic and photoallergic potentials, but many clinical observations have indicated that photosensitivity to KP is a photoallergic reaction with action spectrum of UVA [8]. KP serves as a photohapten because of its photocoupling ability to protein. Our previous studies have shown that KP application plus UVA irradiation induces and elicits photocontact dermatitis in mice, and both $CD4^+$ and $CD8^+$ T cells are required for the full-blown sensitivity reaction [10]. In addition, KP plus UVA upregulates the expression of MHC class II and costimulatory molecules on murine dendritic cells, promoting antigen-presenting ability of the cells [11]. Dendritic cells bearing KP-photoantigen sensitize photoantigen-specific T cells in draining lymph node cells [10].

Avoidance of UVA exposure to the skin site applied with KP prevents photocontact dermatitis. The use of sunscreen UV filters is

* Corresponding author. Tel.: +81 29 837 2460; fax: +81 29 837 0685.
E-mail address: Kenji_Atarashi@hisamitsu.co.jp (K. Atarashi).

1011-1344/$ - see front matter © 2012 Elsevier B.V. All rights reserved.
http://dx.doi.org/10.1016/j.jphotobiol.2012.05.002

one of the common methods for UV protection. In Japan, the patch application is the most popular formulation when KP is topically administered. Employment of UVA filters added to the topical formulations is one of the efficacious strategies to prevent contact photosensitivity. UVA filters can be classified into chemical UVA filters (UV absorbers) or physical UVA filters (UV-scattering nanoparticles). Since UV absorbers convert UV light into the thermal energy, some UV absorbers are photolabile and may have a photosensitive potential. Moreover, it is well known that UVA absorber oxybenzone (benzophenone-3, OX) is photocross-reactive with KP [12–14].

In this study, we investigated the preventive effect of UV filters on KP contact photosensitivity. We first selected an effective UVA filter and tested its ability to suppress the photosensitivity by adding it into the KP patch and gel formulations. Results suggest that the addition of the UVA absorber to topical KP formulations is effective to reduce the photosensitivity without cross-reactivity.

2. Materials and methods

2.1. Animals

Female BALB/c mice (8–10 weeks old) and female Hartley guinea pigs (6 weeks old) were obtained from SLC, Inc. (Hamamatsu, Japan). Female hairless mice (8 weeks old) were obtained from Kudo Co., Ltd. (Tosu, Japan). Male Lewis rats (6 weeks old) were obtained from Charles River Laboratories Japan, Inc. (Yokohama, Japan). All animals were maintained in our animal facility, exposed to a 12 h light: 12 h dark cycle, and provided with food and water *ad libitum*. All animal experiments were performed with the approval of the Laboratory Animal Care and Use Committee at Hisamitsu Pharmaceutical Co., according to Laboratory Animal Welfare guidelines.

2.2. Reagents and topical KP formulations

KP, butyl methoxy dibenzoylmethane (BMDBM) and OX were purchased from Wako Pure Chemical Industries, Ltd. (Osaka, Japan). Diethylamino hydroxybenzoyl hexyl benzoate (DHHB) was purchased from BASF Japan Ltd. (Tokyo, Japan). Hydrophobic particle (mean size: 20 × 100 nm) of titanium dioxide (TiO_2) was purchased from Sakai Chemical Industry Co., Ltd. (Sakai, Japan). All other chemicals were reagent grade or better.

We manufactured two formulations of KP transdermal patch application, i.e. a patch containing BMDBM (BMDBM (+) patch) and a patch non-containing BMDBM (BMDBM (−) patch), by a hot melt method. Both BMDBM (+) and BMDBM (−) patches contained 2% KP. In BMDBM (+) patch, its adhesive layer contained 2% BMDBM, while no UVA filter was added to BMDBM (−) patch. The adhesive layer of both patches consisted of styrene isoprene styrene block copolymer and polyisobutylene, and was laminated on weaved fabric backing. Thickness of the adhesive layer and the fabric backing was approximately 100 and 600 μm, respectively. The other side was covered with a release liner film until use. In addition to the patch application, we also used the gel application, which was Ketum (BMDBM (−) gel) purchased from Menarini France (Rungis, France). To prepare BMDBM-containing KP gel (BMDBM (+) gel), we added BMDBM to Ketum at 1% final concentration and mixed them extensively before use.

2.3. Light source

As UVA source, 40-W black light (FL40SBLB-A) emitting UVA ranging from 320 to 400 nm with a peak emission at 365 nm was purchased from Toshiba Electric Co. (Tokyo, Japan). With a UV radiometer (Topcon Technohouse Corp., Tokyo, Japan), the energy output of eight black light tubes at a distance of 20 cm was 3 mW/cm^2 at 310–400 nm. Irradiation was performed through a pane of 3 mm thickness glass.

2.4. Modified local lymph node assay

Local lymph node assay (LLNA) was performed, as described previously [15], with some modifications to examine photosensitivity. Mice were painted on the dorsal aspect of each earlobe with 25 μL of 2% KP alone or 2% KP plus various concentrations of BMDBM, OX, DHHB or TiO_2 in acetone/olive oil (4:1), and subsequently irradiated with 20 J/cm^2 UVA. The painting plus irradiation was performed on three consecutive days, i.e., days 0, 1 and 2. On day 5, all mice were injected intravenously with 250 μL of phosphate buffered saline (PBS) containing 20 μCi [methyl-^{3}H] thymidine (^{3}H-TdR). Five hours later, the mice were sacrificed, and the draining auricular lymph nodes were removed and pooled for each experimental group. Single cell suspensions of lymph node cells (LNC) were prepared by gentle mechanical disaggregation through cell strainer using the plunger of a syringe. LNC were centrifuged at 1100 rpm for 10 min, washed with 3 mL of PBS and resuspended with 3 mL of 5% trichloroacetic acid (TCA). After overnight incubation at 4 °C, the precipitate was recovered by centrifugation, resuspended with 1 mL of 5% TCA, and transferred to 10 mL of scintillation fluid. ^{3}H-TdR incorporation was measured by β-scintillation counter (Hitachi Aloka Medical, Ltd., Tokyo, Japan). Percentage of control was calculated according to the following formula:

$$\%\ \text{of control} = (\text{sample} - \text{vehicle control})/(\text{KP alone control} - \text{vehicle control}) \times 100.$$

2.5. In vitro skin penetration assay for KP

Penetration of KP through the skin was evaluated by using the Franz diffusion cell system. The diameter of the diffusion cell system used in this study was 2.5 cm, which corresponded to an effective permeable area of 4.9 cm^2. In the mouse skin system, the dorsal skin was excised from sacrificed hairless mice and its fat tissue was removed. In the human skin system, full-thickness human skin samples were obtained from Human and Animal Bridging Research Organization (Tokyo, Japan). After removal of the subcutaneous fat, the skin containing stratum corneum was subsequently sliced using an electric dermatome to 500 μm-thickness materials. Each topical KP formulation was applied to mouse or human skin, and the skin was immediately mounted on the Franz diffusion cell. The receptor chamber was filled with PBS, stirred by a magnetic bar, and maintained at 32 °C. The receptor fluid was flowed at approximately 5 mL/h and collected by an auto-sampler. A part of the collected receptor fluid was mixed with the same volume of acetonitrile. The mixture was centrifuged for 5 min, and the supernatant was transferred into a glass vial. Quantitative analysis of KP was performed on a HPLC Shimadzu-XR (Shimadzu Corp., Kyoto, Japan) equipped with UV detector (254 nm) using a TSK-gel ODS-80Ts column (Tosoh Corp., Tokyo, Japan). The HPLC analysis was performed as follows: the mobile phase, 0.1% acetic acid/acetonitrile; flow rate, 1:1; and injection volume, 20 μL.

2.6. Quantitation of KP and BMDBM in earlobes

Mice were painted with each KP patch formulation on both sides of earlobes for 4 h. After removal of the KP patch, mice were sacrificed, and the earlobes were immediately excised and minced

with surgical scissors. These minces were ground to fine powder by a frost shattering system under liquid nitrogen freezing. The specimens of ground earlobes were placed into a tube at 20 mg. As extraction solvent, 2 mL of methanol was added into the tubes, and the tubes were shaken for 15 min. After centrifugation at 3000 rpm for 10 min, supernatants were transferred to a glass vial. Quantitative analysis of KP was performed as described above. BMDBM was also quantified on a HPLC Shimadzu-XR equipped with UV detector (358 nm) using a TSK-gel ODS-80Ts column. The analysis was performed as follows: mobile phase, 0.1% acetic acid/acetonitrile; flow rate, gradient ratio from 1:1 to 1:20 (1 mL/min), and injection volume, 20 μL.

2.7. KP photostability in topical formulations

After removal of the release liner film, the adhesive aspect of KP patch formulation was irradiated with varying doses of UVA. Residual KP contained in the UVA-irradiated patch was then extracted with tetrahydofuran, and the extracts were diluted with methanol up to a final volume of 50 mL. For the gel formulations, each KP gel was spread on a PET film at 11.4 mg/cm^2 and irradiated with varying doses of UVA. Residual KP contained in the UVA-irradiated gel was extracted with water/methanol (1:1), and the extracts were diluted with methanol up to 50 mL. A part of each extract was filtrated with a pretreatment disk for HPLC (Tosoh Corp.) and transferred into a glass vial. Intact KP was quantified by HPLC as described above.

2.8. Photosensitization and photochallenge to KP in guinea pigs

In our preliminary study, photosensitivity to KP was not induced or elicited in guinea pigs by topical application of KP formulations and subsequent UVA irradiation without adjuvant injection. However, when the adjuvant and strip method as described previously [16] with some modifications was used, KP photosensitivity was detected. By using this method, we investigated the inhibitory effect of BMDBM addition on KP photoallergy. On day 0, guinea pigs were injected subcutaneously with 0.1 mL of emulsified mixture of Freund's complete adjuvant (Wako Pure Chemical Industries, Ltd.) and saline (1:1) at four corners of the application site on the clipped neck (8 cm^2). Each KP patch formulation (8 cm^2) or each KP gel (90 mg) was applied on the neck for 4 h and irradiated with 10 J/cm^2 UVA. The KP application and UVA irradiation to the tape-stripped skin was performed once daily for five consecutive days. In the photosensitization to both KP patch and gel, there were three kinds of application, such as non-application (Group A and B), BMDBM (−) (Group C and D) and BMDBM (+) (Group E and F). On day 21, the guinea pigs were photochallenged with each KP patch (4 cm^2) or KP gel (45 mg) applied for 4 h and subsequent UVA at 10 J/cm^2 on the clipped dorsal skin. In the photochallenge, two skin sites were used for BMDBM (−) (Group A, C and E) and BMDBM (+) (Group B, D and F) formulations. The skin reactions on the photochallenged sites were graded at 24 and 48 h after UVA irradiation according to Draize grading criteria [17]. Erythema and eschar formation are as follows: Score 0, no erythema; Score 1, very slight erythema; Score 2, well-defined erythema; Score 3, moderate to severe erythema; and Score 4, severe erythema to slight eschar formation. Edema formation was as follows: Score 0, no edema; Score 1, very slight edema; Score 2, slight edema; Score 3, moderate edema; and Score 4, severe edema.

2.9. Photosensitization and photochallenge to KP in mice

The mouse model of photocontact dermatitis was described previously [10,18]. Mice were painted with 50 μL of 8% KP, 10% OX or 10% BMDBM in acetone/olive oil (4:1) to the clipped dorsal skin and subsequently irradiated with 40 J/cm^2 of UVA. The painting plus irradiation was performed once daily for three consecutive days. Before photochallenge, the basal line thickness of both ears on all mice was measured with a dial thickness gauge. On day 5, all mice were challenged on both sides of each earlobe with 25 μL of 2% KP, 10% OX or 10% BMDBM in acetone/olive oil (4:1) and subsequently irradiated with 40 J/cm^2 UVA. Ear thickness was measured 24 h after irradiation and was expressed as the mean increment in thickness above basal line control value.

2.10. Chronic inflammatory model

The anti-inflammatory activity of the KP patch formulations was evaluated by using an adjuvant-induced arthritic model [19]. Lewis rats were injected with 0.1 mL of 1% *Mycobacterium butyricum* (Difco Laboratories, Detroit, MI) in liquid paraffin into the left hind paw. On day 14 after the adjuvant injection, each KP patch formulation (1 cm^2) was topically applied to the right hind paw for 24 h, and the application was performed for 7 days. The volume of right hind paw was measured on day 1, 4 and 7 after the first application with a plethysmometer (MK-101CMP; Muromachi Kikai Co., Ltd., Tokyo, Japan). Simultaneously, the edema rate was calculated according to the following formula:

$$\text{Edema rate } (\%) = [(\text{paw volume after adjuvant injection}) / (\text{paw volume before adjuvant injection}) - 1] \times 100.$$

2.11. Statistical analysis

Statistical analysis was performed by Student's *t*-test or Dunnett type multiple comparison using SAS software (SAS Institute Japan Ltd., Tokyo, Japan). *P*-values less than 0.05 were considered to be significant.

3. Results

3.1. Selection of BMDBM as KP-photoprotective agent

In advance of manufacturing UV filter-containing, topical KP formulations, we first compared the potentials of four sunscreen agents to inhibit KP photosensitivity, as assessed by modified LLNA. BMDBM and DHHB are commonly used UVA absorbers, OX is a conventional UV absorber, and TiO_2 is a nanoparticle UV filter. The radio-uptake of draining lymph node cells was measured. Data were expressed as the percentage of control in KP-augmented ^{3}H-TdR incorporation (Fig. 1). The inhibitory effect of BMDBM was strongest among the four filters, especially at a low concentration of 0.25%. Therefore, we chose BMDBM as an UV-protective reagent for topical KP formulations.

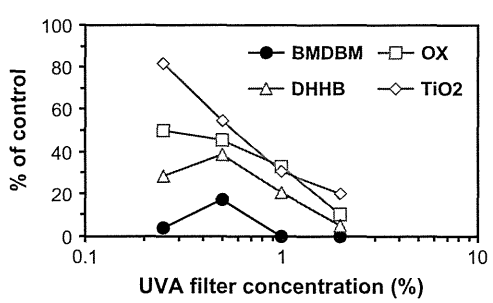

Fig. 1. Inhibitory effects of various UVA filters in organic solvent for KP photosensitivity assessed by murine lymph node proliferation assay.

3.2. No disturbance of KP penetration by BMDBM addition in patch or gel formulation

We examined the skin permeability of KP included in the patch and gel formulations that contained BMDBM [BMDBM (+)] or not [BMDBM (−)]. KP was quantified with HPLC. The cumulative amounts of KP at 12 h in BMDBM (+) patch, BMDBM (−) patch, BMDBM (+) gel, and BMDBM (−) gel were 45.8, 38.5, 15.9 and 14.7 μg/cm^2, respectively (Fig. 2A), without significant differences between BMDBM (+) and BMDBM (−).

To confirm the KP permeability in human skin, each topical KP formulation was applied to the human skin mounted on the Franz diffusion cells, and flowed fluid samples collected by an auto-sampler were quantified with HPLC. Again, the cumulative amount of KP was not significantly different between BMDBM (+) and BMDBM (−) patch formulations (Fig. 2B).

In another experiment, mice were painted with each of the KP patch formulations on both sides of earlobes for 4 h. The earlobes were excised and minced to fine powder by a frost shattering system. Quantitative analyses of KP and BMDBM were performed with HPLC. There was no significant difference in the KP amount between BMDBM (+) and BMDBM (−) patch formulations, while BMDBM was detected in BMDBM (+) but not BMDBM (−) patch (Fig. 3).

3.3. Prevention of photodegradation of KP by BMDBM

The KP photostability in the patch and gel BMDBM (+) formulations irradiated with various amounts of UVA was examined. KP-containing materials were extracted from the irradiated patch and gel formulations, and each extract was quantified for intact KP amount by HPLC. UVA irradiation induced photodegradation of KP in a dose-dependent manner (Fig. 4). The amounts of intact KP in the BMDBM (+) patch and gel were significantly higher than in the BMDBM (−) ones (Fig. 4). Upon exposure to 40 J/cm^2 UVA, intact KP amount was reduced to 26.9% in the BMDBM (−) patch, however, 91.6% of KP remained in the BMDBM (+) patch. Thus, BMDBM effectively protected KP from UVA exposure.

3.4. Suppression of KP photosensitivity by BMDBM in guinea pigs

Guinea pigs were photosensitized and photochallenged with KP patch (Table 1, upper panel) or gel (Table 1, lower panel) formulations and subsequent UVA irradiation. BMDBM was added or not in each KP formulation. Upon challenge, UVA was required for the positive skin reaction (data not shown). In the non-sensitized animals, neither photochallenge with the BMDBM (−) nor BMDBM (+) KP formulation induced responses (Groups A and B). When photosensitized with the BMDBM (−) KP formulation (patch or gel), photochallenge with the BMDBM (−) formulation evoked skin responses (Group C). The gel formulation (lower panel) was more effective than the patch formulation for induction of the sensitivity. However, the BMDBM (+) formulation yielded weaker responses (Group D) than the BMDBM (−) one (Group C). The photosensitized guinea pigs with the BMDBM (+) formulation exhibited weak responses upon challenge with the BMDBM (−) formulation (Group E), but did not show substantial responses with the BMDBM (+) formulation (Group F). Thus, the results indicated that BMDBM effectively depressed the both sensitization and challenge of KP photosensitivity in the guinea pig model.

3.5. No photocross-reaction between KP and BMDBM

It is known that KP photocross-reacts with OX [12–14]. To test the possible cross-reactivity between KP and BMDBM, we used a mouse model of photocontact dermatitis. Mice were photosensitized and photochallenged with KP or OX (Fig. 5A) or with KP or BMDBM (Fig. 5B). Significant ear swelling responses were obtained in KP-photosensitized and photochallenged mice. In this study, as compared to the vehicle sensitization, neither OX (Fig. 5A) nor BMDBM (Fig. 5B) induced significant levels of the photosensitivity. In the KP-photosensitized mice, however, photochallenge with OX elicited a significant response to a lesser degree than photochallenge with KP, suggesting photocross reactivity between KP and OX. On the other hand, photocross reactivity between KP and BMDBM was not observed, as represented by no significant ear

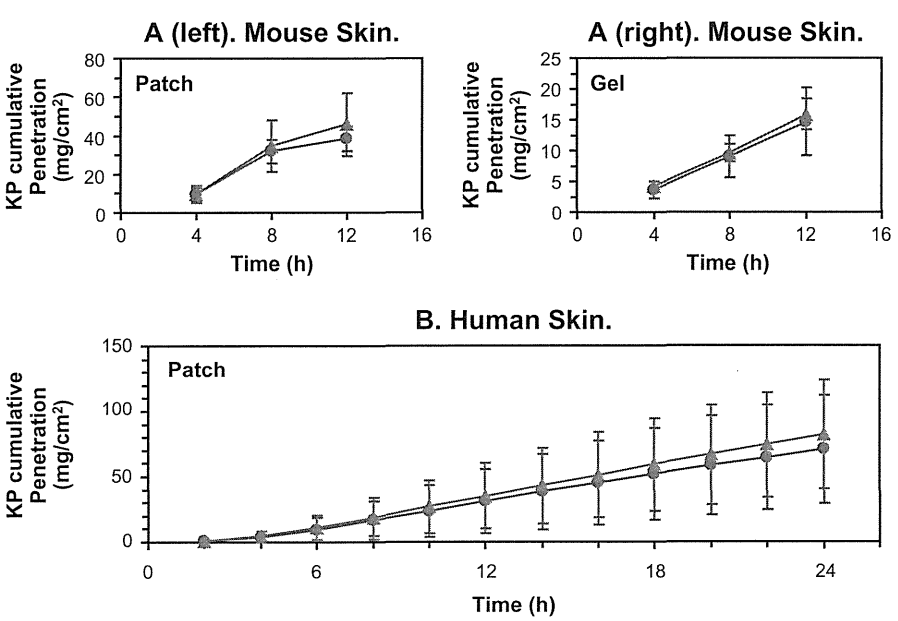

Fig. 2. Effects of BMDBM on KP penetration in topical KP formulations. (A) Data indicate the mean values of KP flux through the mouse skin applied with BMDBM (−) formulation (red circle) or BMDBM (+) formulation (blue triangle). The error bars represent S.D. ($n = 3$). (B) Data indicate the mean values of cumulative KP penetration through the human skin applied with BMDBM (−) patch (red circle) or BMDBM (+) patch (blue triangle). The error bars represent S.D. ($n = 3$). (For interpretation of the references to color in this figure legend, the reader is referred to the web version of this article.)

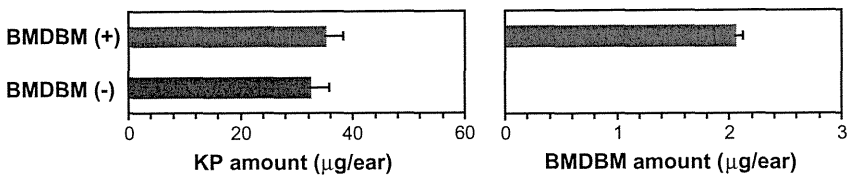

Fig. 3. KP and BMDBM absorption on murine ear from patch formulations. Data indicate the mean values of KP and BMDBM amounts in mouse ear applied with BMDBM (−) patch (red column) or BMDBM (+) patch (blue column). The error bars represent S.D. ($n = 3$). (For interpretation of the references to color in this figure legend, the reader is referred to the web version of this article.)

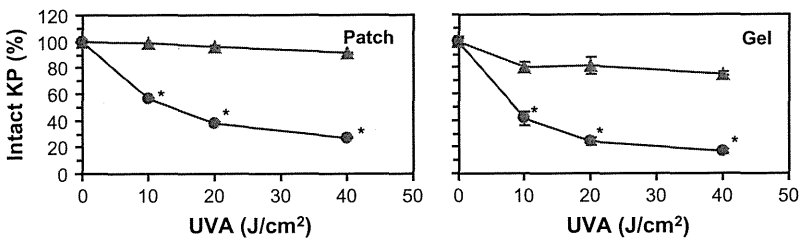

Fig. 4. Inhibitory effect of BMDBM for KP photostability in topical KP formulations. Data indicate the mean values of intact KP percentage in BMDBM (−) formulation (red circle) or BMDBM (+) formulation (blue triangle). The error bars represent S.D. ($n = 3$). Statistical analysis was carried out with Student's *t*-test. (For interpretation of the references to color in this figure legend, the reader is referred to the web version of this article.)

swelling upon photochallenge with BMDBM in KP-photosensitized mice (Fig. 5B).

3.6. No abrogation of the anti-inflammatory ability of KP in BMDBM formulation

We finally compared the anti-inflammatory ability between the BMDBM (+) and BMDBM (−) patch formulations using an adjuvant-induced arthritis rat model. Seven days after beginning of KP application (day 21 after adjuvant injection), the edema rate of hind paw was 95.7% in the positive control without KP (Fig. 6). When applied with the BMDBM (+) and BMDBM (−) formulations, the edema rates were comparably decreased to 60.4% and 50.7%, respectively. This suggested that the anti-inflammatory ability of KP was not abrogated by BMDBM addition.

4. Discussion

Although UVA is the action spectrum of photosensitivity to most of exogenous agents such as KP [8], there are not many available UV filters capable of filtrating UVA wave range. We demonstrated that BMDBM had the strongest potential to reduce KP photosensitivity among the four sunscreen agents tested. In addition, BMDBM (+) patch indicated the similar skin penetration kinetics of KP to BMDBM (−) patch in two different skin studies. Therefore we considered BMDBM was the best UV filter to reduce the photosensitivity to KP patch. It is known that UV absorbers, such as OX, paradoxically can evoke photocontact dermatitis [20–22]. In this respect, UV reflector, as exemplified by TiO_2, is more photostable and less likely to have its photoallergy than UVA absorbers. Although the inhibitory ability of TiO_2 was weaker than BMDBM, we also manufactured a KP patch formulation containing TiO_2. However, the inhibitory effect of TiO_2 addition was not observed in the animal model (data not shown). Since TiO_2 in organic solvent reduced the KP photosensitivity, TiO_2 might be useful as topical formulations such as gel, lotion and cream.

In the present study, significant ear swelling responses of mice photosensitized and photochallenged with 10% BMDBM or 10% OX was not found, while 2% KP significantly induced the photoallergic reactions. Therefore, the photosensitive potentials of BMDBM and OX are greatly lower than that of KP. It has been reported that photocross-reactions occur between KP and other chemicals, such as OX, harbouring a benzophenone moiety [12–14]. We showed that BMDBM was not photocross-reactive with KP in the mouse ear swelling model. In addition, we found using adjuvant and strip method that BMDBM was not photocross-reactivity with KP, while OX cross-reacted with KP (data not shown). From the viewpoint of cross-reactivity, it is also considered that BMDBM is one of the best choices as UVA filter added to KP patch formulations.

KP undergoes a decarboxylation process upon irradiation with UVA in an aqueous solution. Several groups have reported that the main photoproduct of KP formed under an aerobic solution is (3-benzoylphenyl) ethane [23,24]. Photodecarboxylation of KP to (3-benzoylphenyl) ethane proceeds two pathways *via* benzylic carbanion and benzylic radical intermediates [23,25,26]. These radical products from KP might induce covalent binding of KP with protein, when they coexist with each other. Therefore, improvement of KP photostability possibly reduces KP photoallergy. In our study, KP photostability in the topical formulations was significantly elevated by BMDBM addition. It is thought that BMDBM reduces UVA-induced KP decarboxylation and the following formation of radical intermediates.

Table 1
Inhibitory effect of BMDBM in topical KP formulations for KP photosensitivity in guinea pigs.

Group	Photosensitization	Photochallenge	*N*	Mean score	
				24 h	48 h
A	–	BMDBM (−) patch	6	0.0	0.0
B	–	BMDBM (+) patch	6	0.0	0.0
C	BMDBM (−) patch	BMDBM (−) patch	6	1.0	1.2
D	BMDBM (−) patch	BMDBM (+) patch	6	0.7	1.0
E	BMDBM (+) patch	BMDBM (−) patch	6	0.2	0.3
F	BMDBM (+) patch	BMDBM (+) patch	6	0.0	0.3
A	–	BMDBM (−) gel	6	0.0	0.0
B	–	BMDBM (+) gel	6	0.0	0.0
C	BMDBM (−) gel	BMDBM (−) gel	6	3.2	3.5
D	BMDBM (−) gel	BMDBM (+) gel	6	2.0	2.3
E	BMDBM (+) gel	BMDBM (−) gel	6	1.0	1.8
F	BMDBM (+) gel	BMDBM (+) gel	6	0.3	0.7

Mean score indicates an average of total skin reactions graded according to Draize grading criteria [(score of erythema and eschar formation) + (score of edema)].

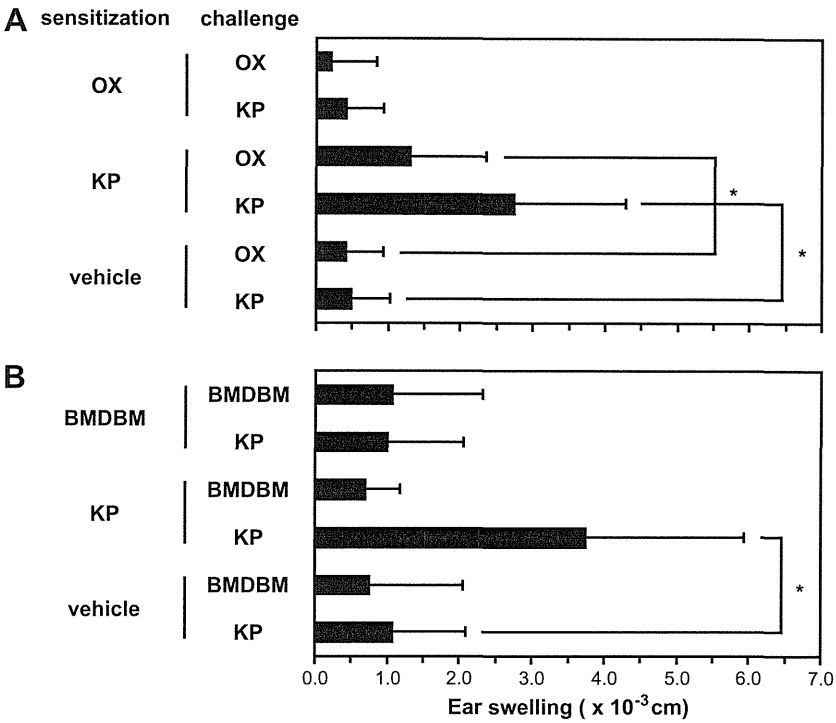

Fig. 5. Cross reactivity of BMDBM to KP in mouse ear swelling test. Mice were photosensitized with 8% KP, 10% OX or 10% BMDBM in acetone/olive oil (4:1) on the clipped dorsal skin. Data indicate mean values of expression as the mean increment in thickness above basal line control value. The error bars represent S.D. ($n = 5$). Statistical analysis was carried out with Student's t-test.

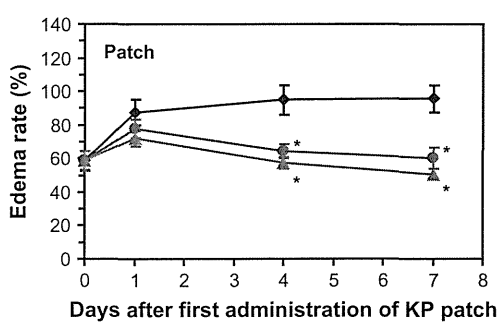

Fig. 6. Anti-inflammatory effect of KP patch formulation containing BMDBM in the adjuvant-induced arthritic model. Data indicate the mean values of edema rate in the rat paw applied with control patch without KP (black diamond), BMDBM (−) patch (red circle) or BMDBM (+) patch (blue triangle). The error bars represent S.E. ($n = 12$). Statistical analysis was carried out with Dunnett type multiple comparison. (For interpretation of the references to color in this figure legend, the reader is referred to the web version of this article.)

Phototreatment with KP induces DNA damage and peroxidation of cell membranes because of radical derivatives and active oxygens [26–28]. The damage reactions to cells cause not only phototoxicity but also photoallergy where immune cells in the skin, such as dendritic cells and keratinocytes, are involved. KP phototreatment upregulates the antigen presenting ability of dendritic cells and promotes the production of cytokines in the epidermis [11]. The photoallergic sensitivity is divided into the photosensitization and the photoelicitation phases. In our mouse KP photocontact dermatitis model [10], we have shown that both KP application and UVA irradiation are mandatory for the sensitivity. In the present guinea pig model, the addition of BMDBM into either sensitization or elicitation formulation successfully reduced the degree of the sensitivity. However, the patients who have already been sensitized with KP should not use even the sunscreen-containing topical formulation. Moreover, although the absorption of BMDBM from patch was fewer than that of KP, in the modified LLNA, the lymph node cell proliferation augmented by KP patch plus UVA was significantly decreased by BMDBM addition (data not shown). In addition, the inhibitory effect of BMDBM addition on KP phototoxicity was also found in mouse ear swelling model (data not shown). Since BMDBM was effective even at a low amount, BMDBM may sufficiently absorb the UV active wavelengths to induce the photosensitivity.

In conclusion, our study demonstrated that BMDBM in topical KP formulations photostabilizes KP and may reduce the photoallergic adverse reaction in clinical use. Photocross-reactivity of BMDBM with KP seems to be absent. The addition of BMDBM does not affect KP permeability and anti-inflammatory activity.

References

[1] Y. Tokura, Photoallergy, Expert Rev. Dermatol. 4 (2009) 263–270.
[2] Y. Iwamoto, T. Itoyama, K. Yasuda, T. Uzuhashi, H. Tanizawa, Y. Takino, T. Oku, H. Hashizume, Y. Yanagihara, Photodynamic deoxyribonucleic acid (DNA) strand breaking activities of enoxacin and afloqualone, Chem. Pharm. Bull. 40 (1992) 1868–1870.
[3] H. Hashizume, Y. Tokura, T. Oku, Y. Iwamoto, M. Takigawa, Photodynamic DNA-breaking activity of serum from patients with various photosensitivity dermatoses, Arch. Dermatol. Res. 287 (1995) 586–590.
[4] Y. Tokura, Quinolone photoallergy: photosensitivity dermatitis induced by systemic administration of photohaptenic drugs, J. Dermatol. Sci. 18 (1998) 1–10.
[5] Y. Tokura, T. Nishijima, H. Yagi, F. Furukawa, M. Takigawa, Photohaptenic properties of fluoroquinolones, Photochem. Photobiol. 64 (1996) 838–844.
[6] Y. Tokura, N. Seo, H. Yagi, F. Furukawa, M. Takigawa, Cross-reactivity in murine fluoroquinolone photoallergy: exclusive usage of TCR Vbeta13 by immune T cells that recognize fluoroquinolone-photomodified cells, J. Immunol. 160 (1998) 3719–3728.
[7] Y. Tokura, M. Ogai, H. Yagi, M. Takigawa, Afloqualone photosensitivity: immunogenicity of afloqualone-photomodified epidermal cells, Photochem. Photobiol. 60 (1994) 262–267.
[8] Y. Tokura, Immune responses to photohaptens: implications for the mechanisms of photosensitivity to exogenous agents, J. Dermatol. Sci. 23 (2000) S6–S9.
[9] T. Yano, A. Nakagawa, M. Tsuji, K. Noda, Skin permeability of various nonsteroidal anti-inflammatory drugs in man, Life Sci. 39 (1986) 1043–1050.

[10] S. Imai, K. Atarashi, K. Ikesue, K. Akiyama, Y. Tokura, Establishment of murine model of allergic photocontact dermatitis to ketoprofen and characterization of pathogenic T cells, J. Dermatol. Sci. 41 (2006) 127–136.
[11] K. Atarashi, K. Kabashima, K. Akiyama, Y. Tokura, Stimulation of Langerhans cells with ketoprofen plus UVA in murine photocontact dermatitis to ketoprofen, J. Dermatol. Sci. 47 (2007) 151–159.
[12] F. Boscá, M.A. Miranda, Photosensitizing drugs containing the benzophenone chromophore, J. Photochem. Photobiol. B 43 (1998) 1–26.
[13] T. Matsushita, R. Kamide, Five cases of photocontact dermatitis due to topical ketoprofen: photopatch testing and cross-reaction study, Photodermatol. Photoimmunol. Photomed. 17 (2001) 26–31.
[14] C.J. Le Coz, A. Bottlaender, J.N. Scrivener, F. Santinelli, B.J. Cribier, E. Heid, E.M. Grosshans, Photocontact dermatitis from ketoprofen and tiaprofenic acid: cross-reactivity study in 12 consecutive patients, Contact Dermatitis 38 (1998) 245–252.
[15] I. Kimber, R.J. Dearman, D.A. Basketter, C.A. Ryan, G.F. Gerberick, The local lymph node assay: past, present and future, Contact Dermatitis 47 (2002) 315–328.
[16] H. Ichikawa, R.B. Armstrong, L.C. Harber, Photoallergic contact dermatitis in guinea pigs: improved induction technique using Freund's complete adjuvant, J. Invest. Dermatol. 76 (1981) 498–501.
[17] J.H. Draize, G. Woodard, H.O. Calvery, Methods for the study of irritation and toxicity of substances applied topically to the skin and mucous membranes, J. Pharmacol. Exp. Ther. 82 (1944) 377–390.
[18] Y. Tokura, H. Yagi, T. Satoh, M. Takigawa, Inhibitory effect of melanin pigment on sensitization and elicitation of murine contact photosensitivity: mechanism of low responsiveness in C57BL/10 background mice, J. Invest. Dermatol. 101 (1993) 673–678.
[19] C.M. Pearson, in: J.L. Hollander, D.J. McCarty (Eds.), Arthritis and Allied Conditions, eighth ed., Lea and Febiger, 1972, pp. 195–207.
[20] A.M. Peluso, F. Bardazzi, A. Tosti, Photocontact dermatitis due to Eusolex 4360, Contact Dermatitis 25 (1991) 65–66.
[21] V. Torres, T. Correia, Contact and photocontact allergy to oxybenzone and mexenone, Contact Dermatitis 25 (1991) 126–127.
[22] R. Silva, L.M. Almeida, F.M. Brandão, Photoallergy to oxybenzone in cosmetic creams, Contact Dermatitis 32 (1995) 176.
[23] S. Monti, S. Sortino, G. De Guidi, G. Marconi, Photochemistry of 2-(3-Benzoylphenyl)propionic acid (Ketoprofen). Part 1. A picosecond and nanosecond time resolved study in aqueous solution, J. Chem. Soc. Faraday Trans. 93 (1997) 2269–2275.
[24] L.L. Costanzo, G. De Guidi, G. Condorelli, A. Cambria, M. Fama, Molecular mechanism of drug photosensitization–II. Photohemolysis sensitized by ketoprofen, Photochem Photobiol 50 (1989) 359–365.
[25] H. Bagheri, V. Lhiaubet, J.L. Montastruc, N. Chouini-Lalanne, Photosensitivity to ketoprofen: mechanisms and pharmacoepidemiological data, Drug Saf. 22 (2000) 339–349.
[26] F. Boscá, M.A. Miranda, G. Carganico, D. Mauleón, Photochemical and photobiological properties of ketoprofen associated with the benzophenone chromophore, Photochem. Photobiol. 60 (1994) 96–101.
[27] M.C. Marguery, N. Chouini-Lalanne, J.C. Ader, N. Paillous, Comparison of DNA damage photoinduced by ketoprofen, fenofibric acid and benzophenone via electron and energy transfer, Photochem. Photobiol. 68 (1998) 679–684.
[28] T. Artuso, J. Bernadou, B. Meunier, N. Paillous, DNA strand breaks photosensitized by benoxaprofen and other non-steroidal antiinflammatory agents, Biochem. Pharmacol. 39 (1990) 407–413.

Published OnlineFirst May 30, 2012; DOI:10.1158/1078-0432.CCR-12-0292

Clinical Cancer Research

Defective Epidermal Innate Immunity and Resultant Superficial Dermatophytosis in Adult T-cell Leukemia/Lymphoma

Yu Sawada, Motonobu Nakamura, Rieko Kabashima-Kubo, et al.

Clin Cancer Res 2012;18:3772-3779. Published OnlineFirst May 30, 2012.

Published OnlineFirst May 30, 2012; DOI:10.1158/1078-0432.CCR-12-0292

Clinical Cancer Research

Defective Epidermal Innate Immunity and Resultant Superficial Dermatophytosis in Adult T-cell Leukemia/Lymphoma

Yu Sawada[1], Motonobu Nakamura[1], Rieko Kabashima-Kubo[1], Takatoshi Shimauchi[2], Miwa Kobayashi[1], and Yoshiki Tokura[2]

Abstract

Purpose: Superficial dermatophytosis is quite commonly seen in patients with adult T-cell leukemia/lymphoma (ATLL), as approximately 50% of the patients develop cutaneous mycotic infections. Because superficially infected fungi in the *stratum corneum* of the epidermis cannot directly contact with T cells infiltrating in the upper dermis, some perturbation of epidermal innate immunity has been postulated. Interleukin (IL)-17–producing helper T cells (Th17) can induce the keratinocyte production of antimicrobial peptides such as human β defensin (HBD)-2 and LL-37, which play an essential role in cutaneous innate immunity.

Experimental Design: We investigated the frequency of circulating Th17 cells, serum levels of cytokines, and epidermal expression of HBD-1, 2, 3, and LL-37 in ATLL patients with or without superficial dermatophytosis.

Results: The frequency of peripheral Th17 cells and the serum level of IL-17 was significantly decreased in ATLL patients, whereas the serum IL-10 and TGF-β1 levels were increased as compared with healthy controls. Furthermore, ATLL patients with dermatophytosis had higher IL-10 and TGF-β1 levels and lower IL-17 levels than did those without dermatophytosis. Immunohistochemical study revealed that the epidermal expression of both HBD-2 and LL-37 were significantly lower in ATLL patients with dermatophytosis than in non-ATLL patients with dermatophytosis.

Conclusions: Taken together, these results suggest that the keratinocyte production of antimicrobial peptides promoted by Th17 cells is reduced in ATLL patients, leading to the perturbed innate immunity and the frequent occurrence of superficial dermatophytosis. *Clin Cancer Res; 18(14); 3772–9. ©2012 AACR.*

Introduction

Adult T-cell leukemia/lymphoma (ATLL) is a malignancy of mature $CD4^+$ T cells caused by human T-cell lymphotropic virus type 1 (HTLV-1; refs. 1–3). HTLV-1 infection is prevalent in southern Japan, especially in Kyushu area (4, 5), Caribbean country, and Africa (6, 7). On the basis of the number of abnormal lymphocytes, organ involvement, and severity, ATLL is divided into 4 clinical categories: acute type, lymphoma type, chronic type, and smoldering type (Shimoyama's classification; ref. 8).

Authors' Affiliations: [1]Department of Dermatology, University of Occupational and Environmental Health, Kitakyushu; and [2]Department of Dermatology, Hamamatsu University School of Medicine, Hamamatsu, Japan

Note: Supplementary data for this article are available at Clinical Cancer Research Online (http://clincancerres.aacrjournals.org/).

Corresponding Author: Yu Sawada, Department of Dermatology, University of Occupational and Environmental Health. 1-1, Iseigaoka, Yahatanishi-ku, Kitakyushu, Japan. Phone: 81-93-691-7445; Fax: 81-93-691-0907; E-mail: long-ago@med.uoeh-u.ac.jp

doi: 10.1158/1078-0432.CCR-12-0292

Superficial dermatophytosis, such as tinea and candidiasis, is quite common in ATLL patients, as approximately 50% of the patients develop cutaneous mycotic infections (9, 10), and the incidence of dermatophytosis of indolent type of ATLL patients was higher than that of aggressive type (10). Dermatophytosis of ATLL patients tended to be intractable even with antifungal treatments, and inflammatory reactions to fungi are less prominent in ATLL patients than non-ATLL dermatophytosis patients (10). These findings have suggested the defective immunity against dermatophytes in ATLL patients. Because superficially infected fungi in the *stratum corneum* of the epidermis cannot directly contact with T cells infiltrating in the upper dermis, some perturbation of epidermal innate immunity has been postulated.

Interleukin (IL)-17–producing helper T (Th17) cells represent a lineage of effector T cells critical in host defense, and dysregulated Th17 cell responses mediate a wide variety of autoimmune and inflammatory conditions such as rheumatoid arthritis (11), inflammatory bowel disease (12), and atopic dermatitis (13). IL-17 stimulates keratinocytes to produce various cytokines, such as granulocyte macrophage colony–stimulating factor, tumor necrosis factor α, CXC

Published OnlineFirst May 30, 2012; DOI:10.1158/1078-0432.CCR-12-0292

Translational Relevance

Adult T-cell leukemia/lymphoma (ATLL) patients often suffer from various infections, such as pneumocystis carinii, pathogenic fungi, viruses, and parasites, and these infections occasionally result in death. Superficial dermatophytosis is quite common in ATLL patients, as approximately 50% of the ATLL patients have tinea, candidiasis, and other cutaneous mycotic infection. However, the pathomechanism of dysfunction of cutaneous innate immunity in ATLL patients remains elusive. Our study clearly showed that Th17 cells play an important role in cutaneous innate immunity. The Th17 cell–enhanced expression of antimicrobial peptides in keratinocytes was decreased in ATLL patients, leading to the perturbed innate immunity and frequent occurrence of superficial dermatophytosis. This is the first step to elucidate the pathomechanism of the impaired cutaneous innate immunity in ATLL patients and to potentially improve the infections and the patients' prognosis.

chemokine ligand 10, and vascular endothelial growth factor (13). IL-17 can also enhance the expression of antimicrobial peptides such as human β defensin (HBD)-2 and LL-37 in keratinocytes (14, 15), which play an essential role in cutaneous innate immunity against fungi. These reports suggested that Th17 cells and IL-17 might play an important role in host defense against superficial dermatophytosis. ATLL cells produce various chemokines and cytokines, such as IL-10 and transforming growth factor (TGF)-β1 (16, 17), which cause immunosuppression in ATLL patients. In particular, IL-10 exerts an inhibitory effect on macrophages and suppresses the cytokine production by Th17 cells (18). In this study, we investigated the frequency of circulating Th17 cells, serum levels of cytokines, and epidermal expression of antimicrobial peptides such as HBDs and LL-37 in ATLL patients.

Materials and Methods

Patient background and clinical evaluation

Eight ATLL patients with dermatophytosis, 7 ATLL patients without dermatophytosis, 6 non-ATLL patients with dermatophytosis, and 8 healthy controls were enrolled in this study. The diagnosis of ATLL was based on the clinical features, histopathologically, cytologically proven mature T-cell malignancy, presence of anti–HTLV-1 antibody, and monoclonal integration of HTLV-1 proviral DNA into blood and/or skin tumor cells as described previously (2, 8, 19, 20). Dermatophytosis was diagnosed with microscopic examinations using KOH preparations. Five of 8 ATLL patients with dermatophytosis had *tinea unguium* in all nails, and 6 patients also had *tinea corporis*. None of the patients took systemic steroids or immunosuppressants. The study design was approved by the review board of University of Occupational and Environmental Health. Skin biopsies and blood examinations were carried out after informed consent had been obtained from the patients. All experiments were conducted in accordance with the Declaration of Helsinki Principles.

Table 1. Statistical analysis of characteristics

	Healthy control	Dermatophytosis	ATLL	ATLL dermatophytosis	*P*
Total	8	6	7	8	
Patient-related factors					
Sex					
Male	5	2	4	4	0.795
Female	3	4	3	4	
Age					
≥70 y	3	2	3	5	0.758
<70 y	5	4	4	3	
Hematologic factor					
Total lymphocyte count					
$\geq 2.0 \times 10^9$/L	2	3	4	2	0.571
$<2.0 \times 10^9$/L	6	3	3	6	
Atypical cells	0	0	2.71 ± 1.38	2.63 ± 2.00	<0.001
PBMC profiles					
CD4/CD8 ratio	1.78 ± 0.77	2.42 ± 1.31	2.68 ± 1.20	4.10 ± 2.05	0.024
$CD4^+CD25^+$ T cells (%)	1.29 ± 0.78	1.59 ± 0.61	2.48 ± 1.25	2.99 ± 1.85	0.051
$CD4^+CCR4^+$ T cells (%)	2.72 ± 1.05	2.84 ± 1.70	3.25 ± 1.22	4.40 ± 2.39	0.222

NOTE: Intragroup comparisons were carried out using the χ^2 test and one-way ANOVA. Each clinical factor showed no statistical differences between each group except the percentage of atypical cells and CD4/CD8 ratio.

Published OnlineFirst May 30, 2012; DOI:10.1158/1078-0432.CCR-12-0292

Patient characteristics

The patients were categorized into 2 groups of age: 70 years or older and younger than 70 years. Lymphocytosis was defined as total lymphocyte count more than 2.0×10^9/L. We also examined the percentage of atypical cells, CD4/CD8 ratio, and percentages of $CD4^+CD25^+$ cells and $CD4^+CCR4^+$ cells.

Flow cytometric analysis of $CD4^+$ T cells, $CD8^+$ T cells, $CD4^+CD25^+$ T cells, and $CD4^+CCR4^+$ T cells

Peripheral blood was obtained by vein puncture from the subjects with heparin as anticoagulant. Peripheral blood mononuclear cells (PBMC) were purified by a standard method using Ficoll-Paque (GE healthcare Bio-sciences AB; ref. 13) and washed twice with PBS containing 2% fetal calf serum (FCS; Thermo Scientific). HBSS containing 0.1% NaN_3 and 1% FCS was used as the staining buffer. After incubation for 30 minutes with monoclonal antibodies (mAb), 10,000 labeled cells were analyzed on a FACSCalibur (Becton Dickinson) in each sample. Fluorescein isothiocyanate (FITC) conjugated mAb to CD4 (SK3) and phycoerythrin (PE) labeled mAb to CD8 (SK1), CD25 (2A3), and CCR4 (1G1) were purchased from BD Immunocytometry Systems.

Intracellular cytokine staining of PBMCs

PBMCs were isolated from patients and control subjects by standard Ficoll-Paque method (Phamacia). Intracellular cytokines were stained according to the protocol of Cytostain (Immunotech) with a few modifications. Cells (2×10^6 cells/mL) were incubated in complete RPMI (RPMI-1640) (Sigma Chemical Co.) containing 10% FCS (Invitrogen), 5×10^{-5} mol/L 2-mercaptoethanol (Gibco), 2 mmol/L L-glutamine (MP Biomedicals), 25 mmol/L HEPES (Cellgro), 1 mmol/L non-essential amino acids (Gibco), 1 mmol/L sodium pyruvate (Gibco), 100 U/mL penicillin (Gibco), and 100 μg/mL streptomycin (Gibco) in a 24-well plate with 10 ng/mL of phorbol-12-myristate 13-acetate (Sigma Chemical Co.), 10^{-6} mol/L of ionomycin (Wako), and 0.7 μL of Goldistop (BD Biosciences) for 8 hours. Then, cells were washed and directly stained with PerCP-conjugated anti-CD8 mAb (BD Biosciences) and subsequently with APC-conjugated anti-CD3 mAb (BD Biosciences) for 20 minutes at 4°C. After washing, 100 μL of Cytofix/Cytoperm buffer (BD Biosciences) was added to each well and incubated for 20 minutes at room temperature and washed with Perm/Wash solution as manufacturer's protocol (BD Biosciences). They were stained with PE-labeled anti-IL17 mAb (BD Bisosciences) for 20 minutes at 4°C. Fluorescence profiles were analyzed by flow cytometry in FACSCanto (BD Biosciences).

Measurement of serum cytokine levels

Peripheral blood samples were transferred to serum separating tubes and centrifuged at $1,000 \times g$ at 20°C for 20 minutes after clot formation. The supernatants were carefully harvested, and aliquots were frozen at −80°C until analysis. The serum IL-17, IL-10, and TGF-β1 levels were measured by ELISA using the Human IL-10 or TGF-β1 Immunoassay Kit (R&D Systems) and the Human IL-17A Immunoassay Kit (eBioscience), respectively, according to the manufacturer's instructions.

Skin biopsy and immunohistochemical staining

Skin biopsy specimens were taken from dermatophytosis lesions of ATLL patients ($n = 8$) and non-ATLL patients ($n = 6$) and from dermatophytosis-unaffected sites of ATLL patients ($n = 7$) and non-ATLL patients ($n = 8$). Formalin fixed, paraffin-embedded tissue sections were first deparaffinized and dehydrated, then washed in TBS (Quartett GmbH) containing 0.1% bovine serum albumin 3 times. Endogenous peroxidase activity was quenched by incubating the slides in a solution of 700 μL H_2O_2 (30%; WAKO) in 70 mL ethanol (WAKO). To carry out antigen retrieval, the sections were pretreated with pepsin (0.4%) for 30 minutes at 37°C. After blocked with normal rabbit or goat serum for 20 minutes, the sections were incubated with 1:50 diluted primary antibody against HBD-1, 2, 3, and LL-37 (Santa Cruz Biotechnology) at room temperature for 60 minutes. The slides were washed in TBS buffer 3 times and incubated with the horseradish peroxidase–conjugated rabbit anti-human IgG or gout anti-human IgG antibody (DAKO) at room temperature for 30

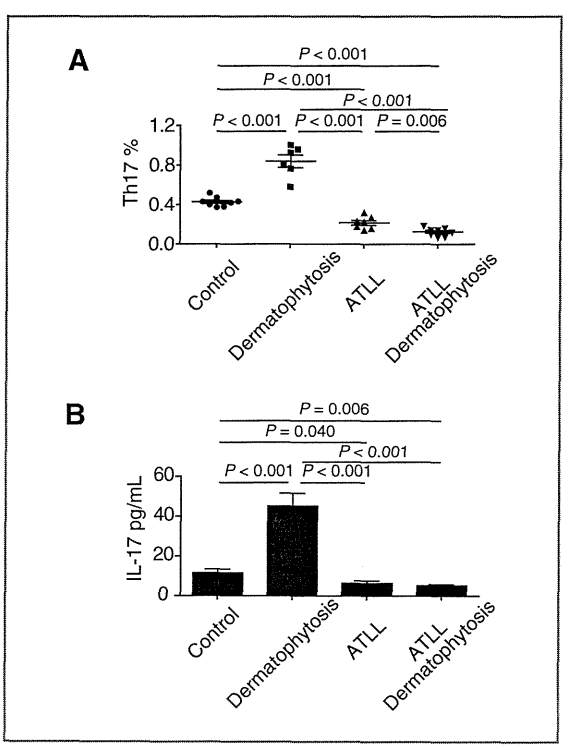

Figure 1. Th17 cell frequencies and IL-17 levels in peripheral blood. A, the percentages of Th17 cells were measured by intracellular IL-17 staining in healthy control, non-ATLL patients with dermatophytosis, ATLL patients without dermatophytosis, and ATLL patients with dermatophytosis. B, the serum IL-17 levels were measured by ELISA.